Science of the Total Environment 650 (2019) 2545–2558

Contents lists available at ScienceDirect

Science of the Total Environment

journal homepage: www.elsevier.com/locate/scitotenv

Pollution characteristics in a dusty season based on highly time-resolved online measurements in northwest China

Fanglin Wang [a], Yunlong Sun [a], Yan Tao [a,*], Yongtao Guo [b], Zhongqin Li [c], Xiuge Zhao [a,d,**], Sheng Zhou [a]

[a] Key Laboratory of Western China's Environmental Systems (Ministry of Education), College of Earth and Environmental Sciences, Lanzhou University, Lanzhou 730000, China
[b] College of Atmospheric Sciences, Lanzhou University, Lanzhou 730000, China
[c] State Key Laboratory of Cryospheric Science/Tien Shan Glaciological Station, Northwest Institute of Eco-Environment and Resources, Chinese Academy of Sciences, Lanzhou 730000, China
[d] State Key Laboratory of Environmental Criteria and Risk Assessment, Chinese Research Academy of Environmental Sciences, Beijing 100012, China

HIGHLIGHTS

- Trace gases and water-soluble ions in PM_{10} were measured based on an online analyzer.
- Pollution characteristics were analyzed in the dust and non-dust period.
- Mixing mechanism was conducted by equivalent ratio analysis in the dust event.
- Sources were identified and quantitated by PMF.
- Potential source-areas were explored by HYSPLIT and CWT.

GRAPHICAL ABSTRACT

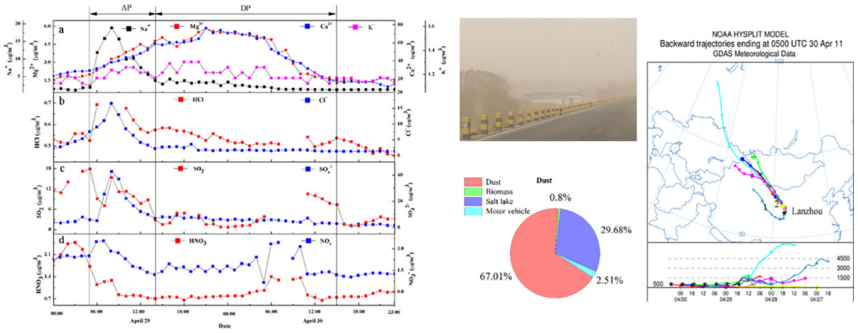

ARTICLE INFO

Article history:
Received 24 July 2018
Received in revised form 28 September 2018
Accepted 30 September 2018
Available online 2 October 2018

Editor: Jianmin Chen

Keywords:
PM_{10}
Dust event
Water-soluble ion
Trace gas
Source apportionment
Potential source-area analysis

ABSTRACT

To investigate the pollution characteristics and potential sources in a dusty season, an online analyzer was used to measure trace gases and major water-soluble ions in PM_{10} from April 1st to May 29th, 2011 in Lanzhou. The average concentrations of HONO, HNO_3, HCl, SO_2 and NH_3 were 0.93, 1.16, 0.48, 9.29 and 5.54 μg/m^3, respectively, and 2.8, 2.76, 8.28 and 2.48 μg/m^3 for Cl^-, NO_3^-, SO_4^{2-} and NH_4^+. In the non-dust period, diurnal variations of SO_4^{2-}, NO_3^- and their gaseous precursors showed similar change trend. NH_4^+ showed unimodal pattern whereas NH_3 illustrated a bimodal pattern. HCl and Cl^- showed an opposite diurnal pattern. In the dust event, temporal profiles of HCl and Cl^-, SO_2 and SO_4^{2-} all presented similar change trend, and SO_4^{2-} and Cl^- preceded dust ions (Ca^{2+} and Mg^{2+}) 13 h. The ratios of NO_3^- to SO_4^{2-} were 0.65 in the non-dust period and 0.31 in the dust event. In the dust event, the sulfur oxidation ratio (SOR) was a factor of 1.33 greater than that in the non-dust period, and $[SO_4^{2-}]/[SO_2]$ was 2.31 times of that in the non-dust period. The source apportionment using Probabilistic Matrix Factorization (PMF) suggested that fugitive dust (58.09%), secondary aerosols (33.98%), and biomass burning (7.93%) were the major sources in the non-dust period whereas dust (67.01%), salt lake (29.68%), biomass burning (0.8%), and motor vehicle (2.51%) were the primary sources in the dust event. Concentration weighted trajectory (CWT) model indicated that NO_3^-, Cl^- and K^+ could be regarded as local source species, the potential sources of Na^+, Mg^{2+} and Ca^{2+} concentrated in the two large areas with the one covered in the junction areas of Xinjiang, Qinghai and Gansu and another one covered the places around in Lanzhou, the potential sources of SO_4^{2-} were mainly localized in the areas adjacent to Lanzhou.

* Corresponding author.
** Correspondence to: X. Zhao, State Key Laboratory of Environmental Criteria and Risk Assessment, Chinese Research Academy of Environmental Sciences, Beijing 100012, China.
E-mail addresses: taoyan@lzu.edu.cn (Y. Tao), hkyzhaoxg@163.com (X. Zhao).

https://doi.org/10.1016/j.scitotenv.2018.09.382
0048-9697/

1. Introduction

Particulate matter (PM_{10}) is an important indicator of air condition and emitted from various natural and anthropogenic activities. PM pollution has aroused the public concerns because it can cause adverse effects on the atmospheric environment, public health, and climate change (Cao et al., 2012a,b; Fang et al., 2016; Hu et al., 2015; Kim et al., 2015; MR et al., 2012; Sun et al., 2014; Ye et al., 2016; Zhang et al., 2015).

Water-soluble ions in PM have been regarded as a crucial factor for its significance in aerosol-phase chemistry reactions and adsorptions of trace gases by particles (Ocskay et al., 2006; Shon et al., 2012; Xue et al., 2011). These major ions include those primary species directly released into the atmosphere and secondary ions formed by oxidation of their corresponding gaseous precursors (SO_2, NOx, and so on) and neutralization with other primary compounds (ammonia, volatile organic compounds, et al.) (Koçak et al., 2015). As an important component of atmospheric aerosols, water-soluble ions affect not only the acidity and formation of aerosols (Han, 2014; Kunwar et al., 2016; C.S. Liang et al., 2016), but also the ecosystems and architectural heritage (T. Liang et al., 2016; Nava et al., 2016). Extensive studies have demonstrated that water-soluble ions occupy a large proportion of PM (Cao et al., 2012a,b; Dao et al., 2014; Du et al., 2011; Tan et al., 2009). In European urban areas, the most abundant water-soluble ions were sulfate and nitrate which could account for 20–30% of PM_{10} mass concentration (Galindo et al., 2013; Putaud et al., 2010; Tolis et al., 2014) whereas in Chinese urban regions, the ratio could be as high as 33% or more (Shen et al., 2011).

Trace gases generally are emitted from natural and anthropogenic sources (Bari et al., 2003; Derwent et al., 2009). It is well-recognized that trace gases like HNO_3, NH_3, HCl, and H_2SO_4 can be converted into aerosols by neutralization and reversible phase equilibrium reactions (Koçak et al., 2015; Seinfeld and Pandis, 2006). HONO also plays an important role in aerosol chemistry as it can be served as a source of OH radicals and its photolysis can lead to 34% comprehensive OH yield in the daytime (Kleffmann et al., 2003; Su and Pöschl, 2011). Previous studies have shown that SO_2 is the most abundant trace gas whereas HCl has the lowest level in the atmosphere (Behera et al., 2013; Kirkby et al., 2011; Kulmala et al., 2000). The average concentrations of N-containing gases (NH_3, HONO and HNO_3) contribute the most in summer and little in winter (Makkonen, 2014).

To identify potential sources of pollutants, several practical receptor models have been developed (Keeler, 1987; Poirot and Wishinski, 1986; Zeng and Hopke, 1989). The most commonly used receptor models are trajectory cluster (Harris and Kahl, 1990; Sirois and Bottenheim, 1995), potential source contribution function analysis (PSCF) (Cheng et al., 1993; Hopke et al., 1993), and concentration weighted trajectory analysis (CWT) (Hsu et al., 2003; Seibert et al., 1994). These models have been widely used by combining meteorology factors, backward trajectories, and concentrations measured at a sampling site. Hybrid Single Particle Lagrangian Integrated Trajectory (HYSPLIT) (Draxler and Hess, 1998) is also frequently used in basic air masses trajectory calculation. A tool named TrajStat has been developed by Wang et al. (2009) which implements cluster calculation, cluster statistics, PSCF, and CWT models into this modeling tool to identify source-receptor relationships.

Lanzhou (35.95° N, 104.14° E), the capital of Gansu Province, is located in a narrow (2–8 km width) and long (40 km) valley basin in Loess Plateau (Fig. 1), which is the home of a large-scale oil refinery and petrochemical industrial base and a key transportation hub in northwestern China. Over the past decades, Lanzhou has been one of the most heavily polluted cities by PM in China and even in the world (WHO, 2014). The severer PM contamination is attributed to frequently occurring stable atmospheric boundary layer and calm winds induced by the mountain-valley topography, arid environment (annual precipitation <300 mm), and massive petrochemical and oil refinery industries. The poor ecological environment and complex topography are uniquely susceptible to the atmospheric pollution, especially high ambient suspended particulate loadings which often take place in spring. The rapid increasing number vehicles in Lanzhou in the past decade further deteriorates the air quality in Lanzhou (Ta et al., 2004; Wang et al., 2006; Wang et al., 2016; Han, 2013). Previously, the investigations into the PM pollution in Lanzhou mostly focused on the pollution levels of PM and its compositions, chemical characteristics, and daily changes in PM concentrations (Pathak et al., 2009; Wang, 2014), there are large knowledge gaps about the relationships between trace gases and water-soluble ions in PM_{10} in a dusty as compared with other cities (Ding et al., 2017; Kulshrestha et al., 2009; Li et al., 2012). Few studies have been carried out to measure trace gases and their related water-soluble ions in PM_{10} during spring, and the temporal variations of water-soluble ions, potential sources, mixing mechanisms and chemical compositions have not been characterized in dust event.

In this article, the observation of trace gases (HCl, HONO, SO_2, HNO_3, and NH_3) and major water-soluble ions (NH_4^+, Na^+, K^+, Ca^{2+}, Mg^{2+}, SO_4^{2-}, NO_3^- and Cl^-) in PM_{10} were performed simultaneously in Lanzhou from April 1st to May 29th, 2011. The present study intends to

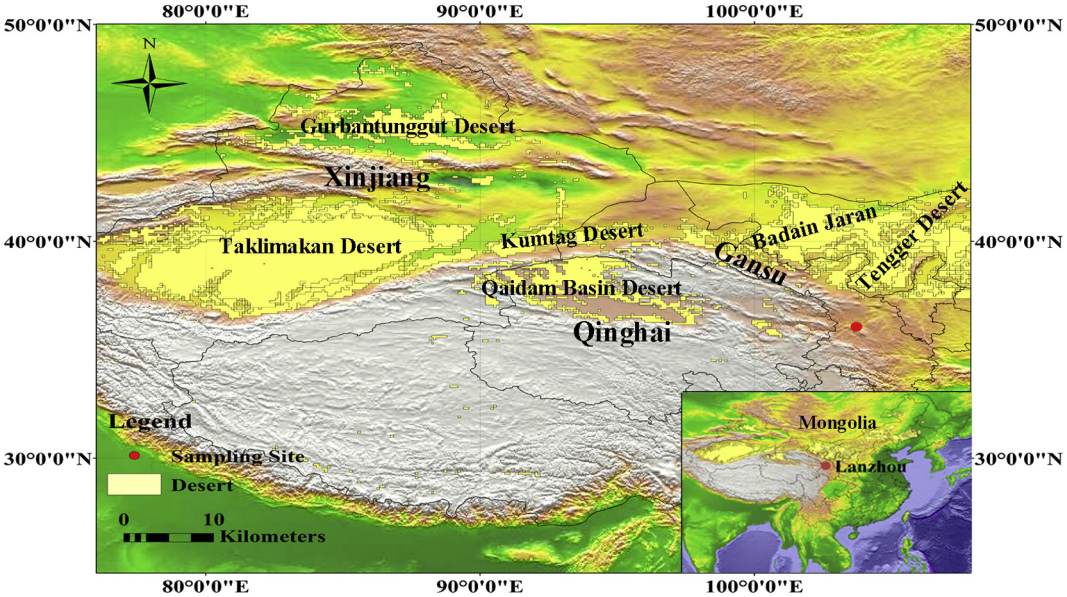

Fig. 1. A map description for locations of sampling site, related Deserts and toponymies.

address three objectives. Firstly, we explored the characterizations of trace gases and water-soluble ions in both dust and non-dust period. Secondly, the relationships between water-soluble ions and their precursor gases and relationships among the water-soluble ions were conducted. Thirdly, the PMF were used to analysis the source apportionment and the HYSPLIT, and CWT models were used to identify major water-soluble ions source regions.

2. Data and methods

2.1. Sampling site

The sampling site (36°03′N, 103°73′E) was chosen on the roof of a two-story building at Lanzhou University, about seven meters above the ground surface, surrounded by residential and commercial settlements. Therefore, the site may reflect a mixed impact from residential, traffic, and construction emissions in an urban region.

2.2. Data resource

A model ADI 2080 online analyzer for Monitoring for AeRosols and Gases (MARGA, Applikon Analytical B.V., Netherlands) (Ten Brink et al., 2007) was employed to obtain gases and ions database from April 1st to May 29th, 2011. More details about MARGA were presented in supplementary material.

The hourly PM_{10} data during the entire observation period was obtained from China National Environmental Monitoring Centre and China Meteorological Data Network, and the hourly meteorological data was obtained from Gansu Meteorological Administration. During the sampling period, a dust event occurred in April 29th and 30th. In the subsequent discussions, we treated these two days as the dust period and the rest of sampling period is regarded as the non-dust period. The data of backward trajectory required in this study were downloaded from HYSPLIT online edition (ftp://arlftp.arlhq.noaa.gov/pub/archives/reanalysis).

2.3. PMF analysis

The source apportionment was analyzed by using the PMF model (version PMF 5.0) (Paatero and Tapper, 2010). The principles and procedures of the PMF are referred to Paatero and Tapper (1994) and Paatero (1997). The general receptor-modeling problem can be written as:

$$\boldsymbol{X} = \boldsymbol{GF} + \boldsymbol{E} \tag{1}$$

where $\boldsymbol{X}$ is the $n \times m$ matrix of ambient element concentrations, $\boldsymbol{G}$ is the $n \times p$ matrix of source contributions, $\boldsymbol{F}$ is the $p \times m$ matrix of source profiles, and $\boldsymbol{E}$ is the matrix of residuals, defined as:

$$e_{ij} = X_{ij} - \sum_{k}^{p} g_{ik} f_{kj} \tag{2}$$

where $i = 1, \ldots, n$ is the number of samples; $j = 1, \ldots, m$ is the number of elements; $k = 1, \ldots, p$ is the number of sources.

The aim of PMF is to minimize the object function $Q(E)$ under relatively constant condition by running many times with different *Fpeak* (Lee et al., 2003b; Norris, 2014), the objective function $Q(E)$ based on the uncertainties inherent is applied as follows:

$$Q(E) = \sum_{i=1}^{n} \sum_{j=1}^{m} \left(\frac{e_{ij}}{s_{ij}} \right)^2 \tag{3}$$

where s_{ij} is the uncertainty estimate in the jth element measured in the ith sample, and the uncertainty (Unc) is calculated as follows (Norris, 2014; Polissar et al., 2001; Reff et al., 2007):

$$Unc = \frac{5}{6} \times MDL (C \le MDL) \tag{4}$$

$$Unc = \sqrt{(RSD \times C)^2 + (0.5 \times MDL)^2} (C > MDL) \tag{5}$$

where RSD is the relative standard deviation, C is the concentration of element, μg/m^3, and MDL is the method detection limit. In this study, seven measured water-soluble ions in the dust event and eight measured water-soluble ions in the non-dust period were chosen as the input data to the PMF 5.0, and all the water-soluble ions residuals ranged from −2 to 2. The observed and calculated from PMF of total water-soluble ion showed higher correlations ($R^2 = 0.99$ for the dust event, $R^2 = 0.96$ for the non-dust period) (Fig. S4), more details about mathematical diagnostics for the results were itemized in supplementary material.

2.4. Backward trajectory analysis

Backward trajectories of air masses arriving in Lanzhou were calculated using the HYSPLIT developed by the National Oceanic and Atmospheric Administration (NOAA). By using the HYSPLIT, possible trajectories of atmospheric pollutants could be calculated and analyzed (Draxler and Hess, 1998; Sirois and Bottenheim, 1995). In this paper, 48-h backward trajectory of air masses and trajectory cluster analysis were carried out based on the GIS-based software TrajStat (Wang et al., 2009). The trajectory height was set 500 m (above the ground level) because the winds at this height can effectively reduce the influence of ground surface friction and more accurately reflect the characteristic of the mean flow field in the atmospheric boundary layer (Wang et al., 2009).

2.5. Concentration weighted trajectory analysis

To identify potential sources and their relative importance, the weighted trajectory associated with measured pollutant concentrations, named CWT, was employed (Hsu et al., 2003). In this model, each grid cell is assigned a weighted concentration obtained by averaging the concentration of corresponding trajectory crossed the grid:

$$C_{ij} = \frac{1}{\sum_{l=1}^{M} \tau_{ijl}} \sum_{l=1}^{M} C_l \tau_{ijl},$$

where, C_{ij} is the average weighted concentration in the ijth cell, l is the index of the trajectory, M is the total number of trajectories, C_l is the concentration observed on arrival of trajectory l and τ_{ijl} is the time spent in the ijth cell by trajectory l. In this study, the areas (80°E-110°E, 30°N-45°N) covered by backward trajectories were incised into 0.5° × 0.5° grids. The sampling site (35.95°N, 104.14°E) was set as CWT's target point. The mean concentration averaged over the model domain was selected as a threshold to identify both moderate and major sources.

CWT is a conditional probability function and the uncertainty of CWT value increase when the air flow delays in a short time in some grids (n_{ij} value is smaller). To reduce uncertainty, W_{ij} (weighting factor) is introduced (Polissar et al., 2001) when all trajectory points in a grid are <3 times of the average trajectory endpoints at each grid in the study area. The weight function is as follows:

$$W_{ij} \begin{cases} 1.00 & n_{ij} > 3Avg \\ 0.70 & Avg < n_{ij} \le 3Avg \\ 0.42 & 0.5Avg < n_{ij} \le Avg \\ 0.17 & 0 < n_{ij} \le 0.5Avg \end{cases},$$

$$WCWT_{ij} = C_{ij} \times W_{ij},$$

where n_{ij} is the number of endpoints that fall in the *ij*th cell, *Avg* is the average number of endpoints for all grids in the study area.

3. Results and discussion

3.1. Characteristics of trace gases and water-soluble ions during the dust event and non-dust period

Temporal variations of visibility and daily average concentrations for measured species were showed in Fig. 2. In the non-dust period, the average visibility was 34.04 km and the daily PM_{10} concentrations ranged from 52.00 to 286.71 μg/m^3, and the mean value was 152.70 ± 58.67 μg/m^3. A total of 29 PM_{10} pollution days was identified with 24-hour average value exceeding the Chinese Ambient Air Quality Secondary Standard (150 μg/m^3, GB 3095-2002). For the ionic concentrations (Fig. 2, Table S1 and Fig. S1), Ca^{2+} exhibited the highest concentration among all water-soluble ions analyzed, with daily average concentration at 17.93 ± 8.76 μg/m^3, which accounted for 50.91% of water-soluble ions and 13.03% of PM_{10}, followed by secondary soluble ions including SO_4^{2-} (7.07 ± 4.53) μg/m^3, NO_3^- (3.56 ± 1.94) μg/m^3, and NH_4^+ (2.48 ± 2.37) μg/m^3. These secondary ions together accounted for 36.03% of water-soluble ions and 8.25% of PM_{10}. Higher concentration of SO_4^{2-} was observed from April 1st to 16th. Although the coal heating of Lanzhou was terminated on March 31st as the reaction between SO_2 and OH could extend from 7 to 14 days during the formation of SO_4^{2-} (Finlayson-Pitts, 2009; Jacob, 1999). For the trace gases (Fig. 2, Table S1 and Fig. S2), the mean concentrations of SO_2 and NH_3 were as high as 12.88 ± 16.29 μg/m^3 and 7.86 ± 5.97 μg/m^3, respectively, constituting the majority (87%) of the total trace gases. On the other hand, HCl level was very low and hence could be ignored. The averaging concentrations of all species in daytime and nighttime during the non-dust period were illustrated in Table S1 and Fig. S3. The concentrations of SO_2, SO_4^{2-}, NH_3, NH_4^+, and NO_3^- were much higher in the daytime than those in the nighttime, indicating that human activities influenced these pollutants. Cl^- and Ca^{2+} showed relatively high concentration in the daytime as well whereas other contaminants had no obvious difference between the daytime and nighttime.

In the two-day dust event, the visibilities were 8.0 km and 17.1 km, respectively. The average concentration of water-soluble ions increased to different levels compared with those before and after the dust event except for NH_4^+ due to the instrument error. The increases of SO_4^{2-}, Cl^-, Na^+, Mg^{2+} and Ca^{2+} were particularly significant. Among which Ca^{2+} had the highest level, increasing dramatically with the massive intrusion of dust characterized by high level of calcium carbonate ($CaCO_3$) (Huang et al., 2010a,b). $CaCO_3$ forms an important part of crust and contributes most to the soil and aerosols in northwest China (Wang et al., 2008, 2012). Except for HCl, the daily concentrations of trace gases were lower than those sampled before and after the dust event. This might be attributed to strong winds which could blow atmospheric pollutants away from the sampling site.

3.2. Diurnal variation of meteorological factors, water-soluble ions, and trace gases during the dust event and non-dust period

The diurnal variations of the mean wind speed, temperature, and relative humidity during the non-dust period were depicted in Fig. 3. The diurnal change in the temperature showed unimodal pattern with the minimum at 06:00 LT (local time, hereafter) (6.25 °C) and

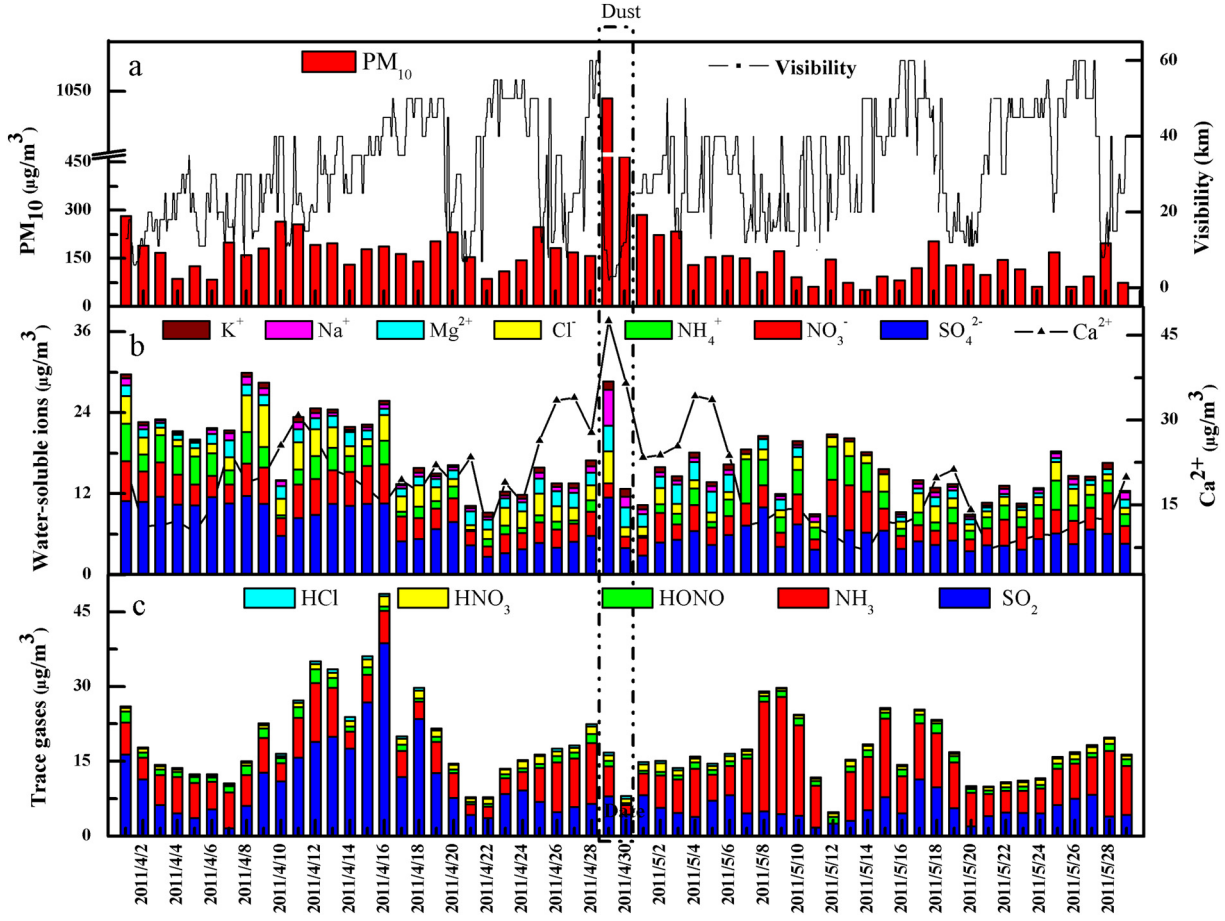

Fig. 2. Temporal variations of PM_{10} and visibility (a), water-soluble ions (b) and trace gases (c) during the whole campaign (Species inside the rectangle represent the dust event occurring in April 29th and 30th).

the maximum occurring at 16:00 LT (17.96 °C). The diurnal variation of the relative humidity was opposite to the temperature with the maximum occurring in the early morning and the minimum occurring in the afternoon. The wind speed increased monotonically from 07:00 to 17:00 LT with the peak at 17:00 LT and then decreased thereafter. Overall, the increasing wind speed and temperature and decreasing humidity were observed in the daytime, and vice versa during the nighttime.

As showed in Fig. 4a, diurnal variation of NH_3 showed bimodal pattern with one peak at 09:00 LT. The other occurred at 19:00 LT. The major sources of NH_3 in the urban atmosphere were traffic emission and combustion (Battye et al., 2003; Sutton et al., 2000). Considering its diurnal variation, the traffic emission might play a more important role in NH_3. Due likely to the different distance between the sampling site and the roads in the present study as comparing with some previous studies (e.g., Whitehead et al., 2007), the diurnal pattern of NH_3 in our case differed from other cities (Hesterberg et al., 1996; Trebs et al., 2004). NH_4^+ was formed by the reactions of NH_3 with acid trace gases in humid aerosols, it exhibited a unimodal pattern with the maximum at 10:00 LT, and then decreased thereafter till to 19:00 LT, which might be attributed to the increasing temperature because NH_4NO_3 and NH_4Cl could volatilize easily as explained by following chemical reaction (Seinfeld and Pandis, 2006):

$$NH_4NO_3 \rightarrow NH_3 + HNO_3,$$
$$NH_4Cl \rightarrow NH_3 + HCl.$$

The increase of the boundary layer height might be another reason for the decrease of NH_4^+ during the daytime (e.g., 10:00–19:00 LT, Trebs et al., 2004).

Fig. 4b shows the diurnal variations of SO_2 and SO_4^{2-}. SO_2 and SO_4^{2-} illustrated similar temporal variations and their trends could be explained by a unimodal pattern. The maximum of SO_4^{2-} occurred at 9:00 LT and remained a relatively high concentration from 06:00 to 16:00 LT. The higher oxidation capacity substance such as OH radical and O_3 in Lanzhou could enhance the conversion of SO_2 to SO_4^{2-} during the daytime (Du et al., 2011).

Diurnal variations of HCl and Cl^- are showed in Fig. 4c. HCl concentration increased from 8:00 LT and peaked at 14:00 LT, and decreased gradually thereafter. The diurnal pattern of Cl^- showed an opposite trend to HCl. The Cl^- formation can be explained by:

$$HCl + NH_3 \rightarrow NH_4Cl,$$

hence, decreasing HCl corresponds to the increasing Cl^-. The primary emissions of HCl include coal combustion and waste incineration (Biswas et al., 2008) whereas its secondary source could be attributed to follow reactions (Eldering et al., 1991):

$$HNO_3 + NaCl(sea\ salt) \rightarrow NH_4Cl + HCl \quad (1)$$

$$NH_4Cl \rightarrow NH_3 + HCl. \quad (2)$$

Considering the surroundings of the sampling site and the diurnal variation of HNO_3 (Fig. 4d), we may assume that HCl was mainly came from coal combustion, waste incineration, and evaporation of NH_4Cl. The decreased Cl^- was resulted from the second reaction (2) mechanism.

As showed in Fig. 4d, HONO had its highest concentration at 07:00 LT and decreased thereafter till 17:00 LT with higher concentration in the nighttime. The heterogeneous reaction of NO_2 ($NO_2 + H_2O \rightarrow HONO + HNO_3$) is an important source of HONO (Heland et al., 2001). Under the relatively higher relative humidity and lower boundary layer height during the nighttime, HONO might be formed and accumulated in night. The decreasing HONO in the daytime might been caused by its photolysis reaction ($HONO + h\nu \rightarrow NO + OH$) (Bari et al., 2003). HONO plays a very important role in the formation of secondary pollutants since it is one of the most important oxidants in the troposphere.

HNO_3 shows almost the same diurnal change as HONO. The photochemical reaction of NO_x ($NOx = NO_2(g) + NO(g)$) was a main source of HNO_3 (Lin et al., 2006). In the daytime, HNO_3 was formed by the photochemical reaction of NO_2 with OH (Seinfeld and Pandis, 2006):

$$NO_2(g) + OH + M \rightarrow HNO_3(g) + M.$$

During the nighttime, HNO_3 can be formed by the following reactions (Jacob, 1999):

$$NO_2(g) + O_3(g) \rightarrow NO_3(g) + O_2(g)$$
$$NO_3(g) + NO_2(g) + M \rightarrow N_2O_5(g) + M$$
$$N_2O_5(g) + H_2O \rightarrow 2HNO_3(g).$$

NO_3^- illustrates the similar diurnal variation as NH_4^+ with increasing concentration after sunrise (06:00 LT) and reaches its highest value at 10:00 LT, and then began to decrease, indicating that these two ions have the same formation pathway as follows:

$$HNO_3 + NH_3 \rightarrow NH_4NO_3.$$

NH_4NO_3 is a semi-volatile species (Mozurkewich, 1993), which increases with the increasing temperature and decreasing the concentration of NO_3^-.

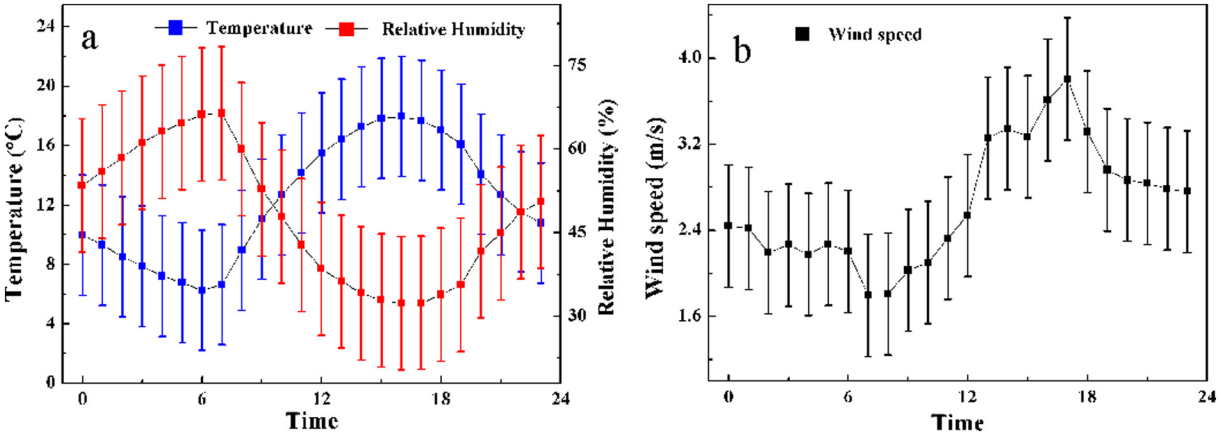

Fig. 3. Diurnal variations of temperature and relative humidity (a) and wind speed (b) during the non-dust period (the vertical bar denotes their respective standard deviation).

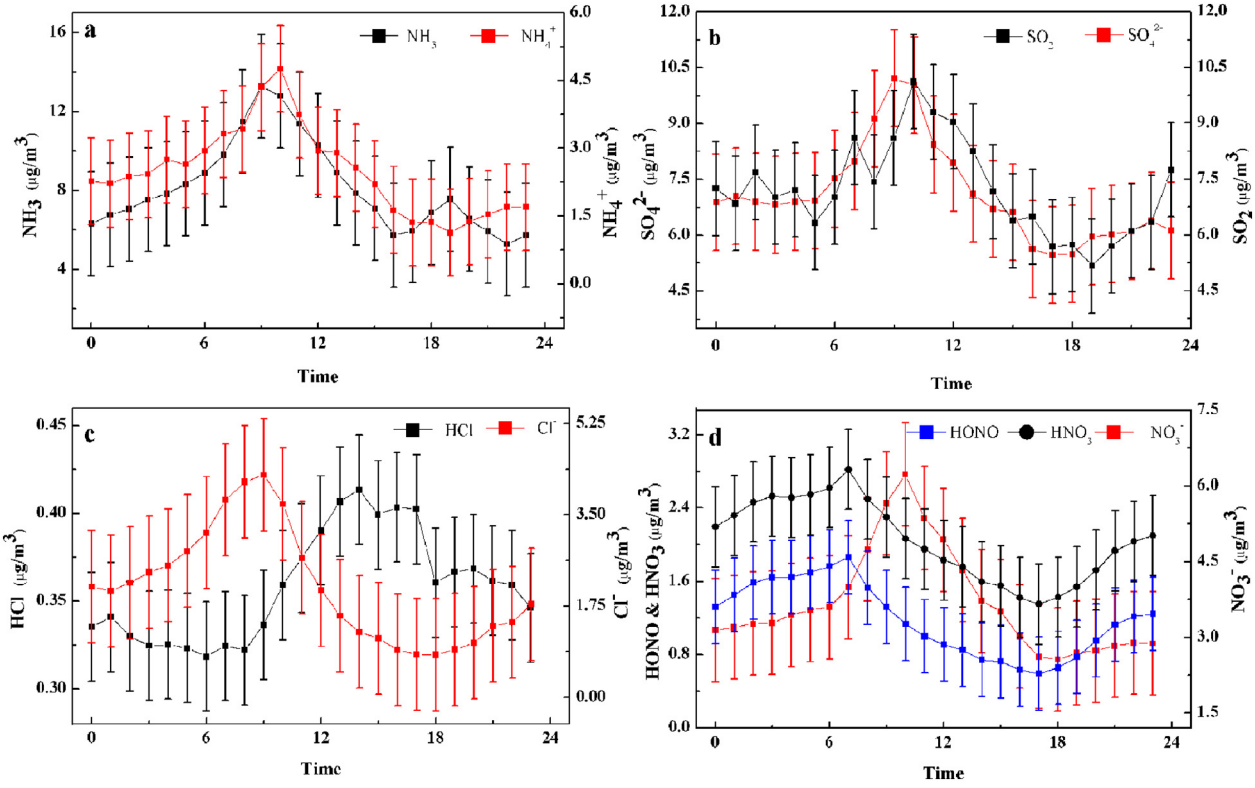

Fig. 4. Diurnal variations of trace gases (black square) and their corresponding water-soluble ions (red square) during the non-dust period (blue square represents HONO, the vertical bar denotes their respective standard deviation).

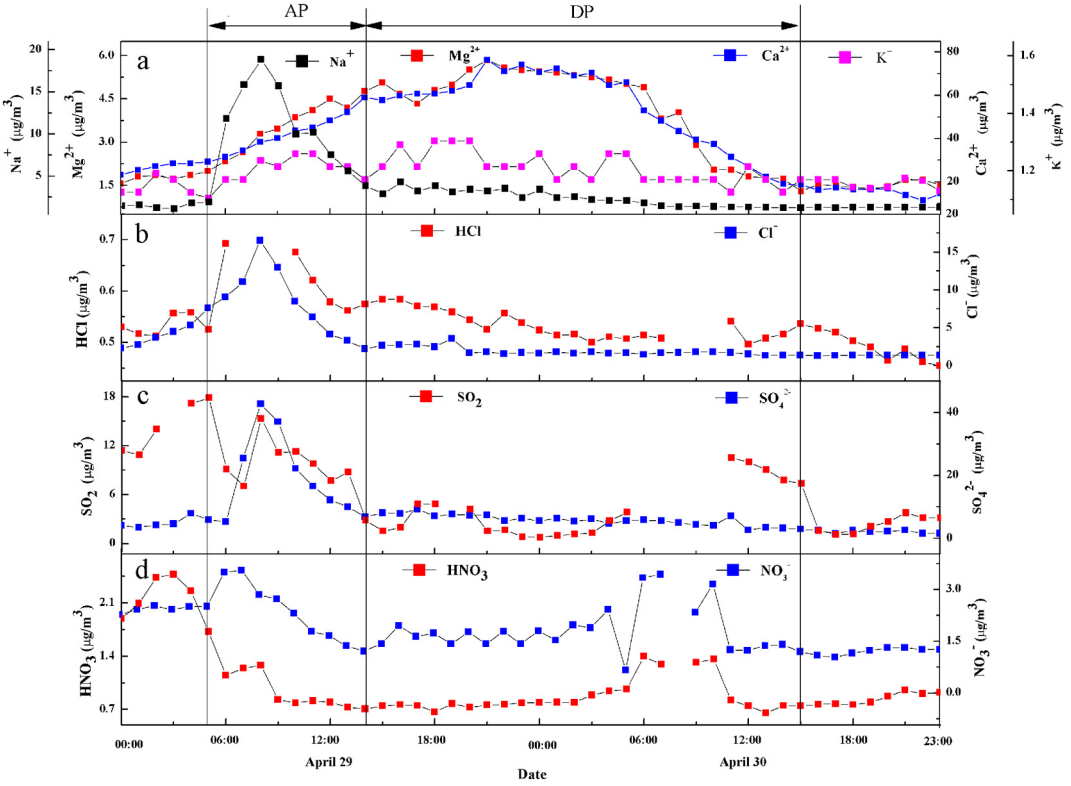

Fig. 5. Temporal profiles of cation ions (a), and water-soluble ions and corresponding trace gases (b, c, d) (blue square represents water-soluble ion, red square represents trace gas) in the dust event (the anthropogenic-dominant period and dust-dominant period are marked between the lines as 'AP' and 'DP', respectively).

The diurnal variations of water-soluble ions and trace gases in the dust event are depicted in Fig. 5, in which the anthropogenic-dominant period and dust-dominant period were defined by 'AP' and 'DP', respectively. The temporal profiles of Na^+, HCl and Cl^-, SO_2, and SO_4^{2-} show similar fluctuations and exhibit a "Λ" pattern with their peak values at 08:00 LT (AP), so did Mg^{2+} and Ca^{2+}, these chemicals reached their maximums (DP) after 13 h from 08:00 LT, indicating that preliminary pollutants from AP and DP were not necessarily transported together and did not mix with each other. The result was in line with that from some studies in other locations (Bates et al., 2004; Choi et al., 2008; Hatakeyama et al., 2004; Matsumoto et al., 2003; Uematsu et al., 2002; Wang et al., 2013; Zhang et al., 2005). However, our result disagreed with those cases in which sulfate and nitrate were formed by heterogeneous reactions during the course of long-range transport and well mixed anthropogenic pollutants and dust particles (Formenti et al., 2010; Huang et al., 2010b; Ndour et al., 2008; Usher et al., 2003).

In the AP, SO_2 and SO_4^{2-} were higher than that in the DP. The peak concentration of SO_4^{2-} was 42.75 μg/m^3 and accounted for 37% of the total measured water-soluble ions. As SO_2 can be transported for hundreds of kilometers before its reaction (oxidation) if the weather conditions are unfavorable for its oxidation or the oxidizing substance were insufficient in the air, such the long-range transport might play more significant role in the change in SO_2 (Erduran and Tuncel, 2001). The contribution of fugitive dust should also not be overlooked as it has been reported that the background concentration of SO_4^{2-} could be as high as 1.4 mg/g in typical salty soil in North China (Jiang and Zhang, 2011).

HCl and Cl^- followed basically the same trend in AP and DP, respectively. The temporal fluctuations of Cl^- and Na^+ were the same as SO_4^{2-} and also occurred during the AP, indicating that they might have the same source. The concentration of Na^+ ranged from 1.21 μg/m^3 to 18.81 μg/m^3 and Cl^- ranged from 1.35 μg/m^3 to 16.55 μg/m^3, respectively. Their peak values were 17.42 and 8.15 times higher than those average values in the non-dust period. There are many dried salt lakes in the northern and northwestern China in which NaCl and some other salts are common components (Zheng, 1991). Therefore, it could be deduced that the following reactions contributed the concentration of Cl^-:

$$NaCl + HNO_3 \rightarrow HCl + NaNO_3$$
$$NH_3 + HCl \rightarrow NH_4Cl.$$

The mole ratio of Na^+ to Cl^- was 1.74, indicating that the source of Na^+ contained not only salt lakes but also local dust.

In the DP, the peak concentration of Ca^{2+} was 76.34 μg/m^3, contributing 78% to the total measured water-soluble ions alone. The highest concentration of Mg^{2+} was 5.84 μg/m^3, 4.17 times of the average value in the non-dust period. The temporal profiles of Ca^{2+} and Mg^{2+} manifest that that large amount of Ca^{2+} and Mg^{2+} measured in Lanzhou came from Gobi Deserts or Deserts through long-range transport and deposition, because Ca^{2+} is one of the most common mineral salts in the surface soil in the Taklamakan Desert, Gobi Deserts, and Loess Plateau (Li et al., 2007; Maher et al., 2009). Due to this fact, Ca^{2+} is usually chosen as a tracer of dust (Huang et al., 2010a,b; Wang et al., 2012). Some studies revealed that the molar ratio of Mg^{2+} to Ca^{2+} was 0.15 in the northern deserts and loess topsoil of China (Osada et al., 2002). In this study, the molar ratio of Mg^{2+} to Ca^{2+} was 0.15 in the DP, agreeing well with their ratio in deserts and loess, further demonstrating that Mg^{2+} and Ca^{2+} had the same sources in Gobi-deserts or Loess Plateau.

The temporal variations of K^+, HNO_3, and NO_3^- had no significant change in the AP and DP during the dust event. As a tracer of biomass burning (Dibb et al., 1996; Duan et al., 2004; Liu et al., 2000; Ma et al., 2003), the presence of K^+ in measured samples suggest that biomass burning did not occurred in the dust event, but it might be conveyed from the upwind sources because its concentration increased slightly in both AP and DP. Likewise, although there was no obvious difference of HNO_3 and NO_3^- between the AP and DP, their concentration changes were the same as those in the non-dust period.

3.3. Mixing mechanisms

In the non-dust period, according to Spearman correlation coefficients (SCCs) analysis of water-soluble ions (Table S2), the predominant salts were: NH_4NO_3 ($r = 0.662$, $p < 0.01$), KCl ($r = 0.420$, $p < 0.01$) and $(NH_4)_2SO_4/NH_4HSO_4$ ($r = 0.756$, $p < 0.01$) (Table S2).

In the dust event, there existed complicated combination between cations and anions. To understand possible cation-anion associations among water-soluble ions, an equivalent ratio analysis was conducted. The results were showed in Fig. 6. In the figure, R^2 and S represented the regression coefficient and the slope of the linear regression equation, respectively. The linear regression coefficient suggested that SO_4^{2-} was strongly associated with Na^+ ($R^2 = 0.96$, S = 1.42), but no association with Ca^{2+}, Mg^{2+}, and K^+. The result implied that Na_2SO_4 was a major combination. As NO_3^- had no association with any cation ions, we inferred that it might be associated with NH_4^+, similar to that in the non-dust period. Cl^- had a strong correlation with Na^+ ($R^2 = 0.65$, S = 0.39), indicating the presence of NaCl. In this study, the balance of overall ions was not illustrated since there was a large cation excess. To explore the cation excess that might be resulted from the lack of CO_3^{2-} measurement which apparently was attributed to the presence of $CaCO_3$ (Lee et al., 2003; Maxwell-Meier et al., 2004), we assumed that the particles were charge-neutral and the CO_3^{2-} was the only unmeasured anionic (Weber et al., 2005), then the CO_3^{2-} ($[CO_3^{2-}]$ estimated) could be estimated by subtraction of the total measured anion equivalence from total measured cation equivalence as follows:

$$\left[CO_3^{2-}\right]_{\text{estimated}} = \sum_i^n [\text{Cation}]_{measured,i} - \sum_j^m [\text{Anion}]_{measured,j},$$

where n and m stand for the total number of cations and anions measured by MARGA, as showed in Fig. 7. The estimated CO_3^{2-} concentration was almost perfectly associated with Ca^{2+} ($R^2 = 0.98$, S = 1.06) and Mg^{2+} ($R^2 = 0.94$, S = 15.86), indicating that dust particle remained intact over the long-range transport and the CO_3^{2-} were not replaced by SO_4^{2-} or NO_3^-.

3.4. Ratio analysis of measured species

3.4.1. $[NO_3^-]/[SO_4^{2-}]$

SO_2 is mainly produced from stationary sources such as coal combustion and is the main precursor of SO_4^{2-}. NOx is mainly released from the mobile sources and is the main precursor of NO_3^-. To assess the relative importance of mobile and stationary sources, the mass ratio of NO_3^- to SO_4^{2-} is often used. The higher $[NO_3^-]/[SO_4^{2-}]$ indicates the advantage of mobile sources over stationary sources, and vice versa (Arimoto et al., 1996).

The mean mass ratios of NO_3^- to SO_4^{2-} were 0.56 in the non-dust period and 0.31 in the dust event, confirming that the stationary sources contributed more to the PM pollution than mobile sources, either in the non-dust period or in the dust event. The ratio in the dust period was a factor of 1.8 lower than that in the non-dust period, indicating higher SO_4^{2-} in the dust event.

3.4.2. SOR and $[SO_4^{2-}]/[SO_2]$

The SOR ($SOR = SO_4^{2-} / (SO_4^{2-} + SO_2)$) is the ratio of SO_4^{2-} to the total sulfur, reflecting the degree of transformation from SO_2 to SO_4^{2-} (Lin, 2002). It has been reported that SOR was smaller than 0.1 when SO_4^{2-} was emitted from primary sources whereas SOR was above 0.1 when SO_4^{2-} was mainly produced through the secondary formation of

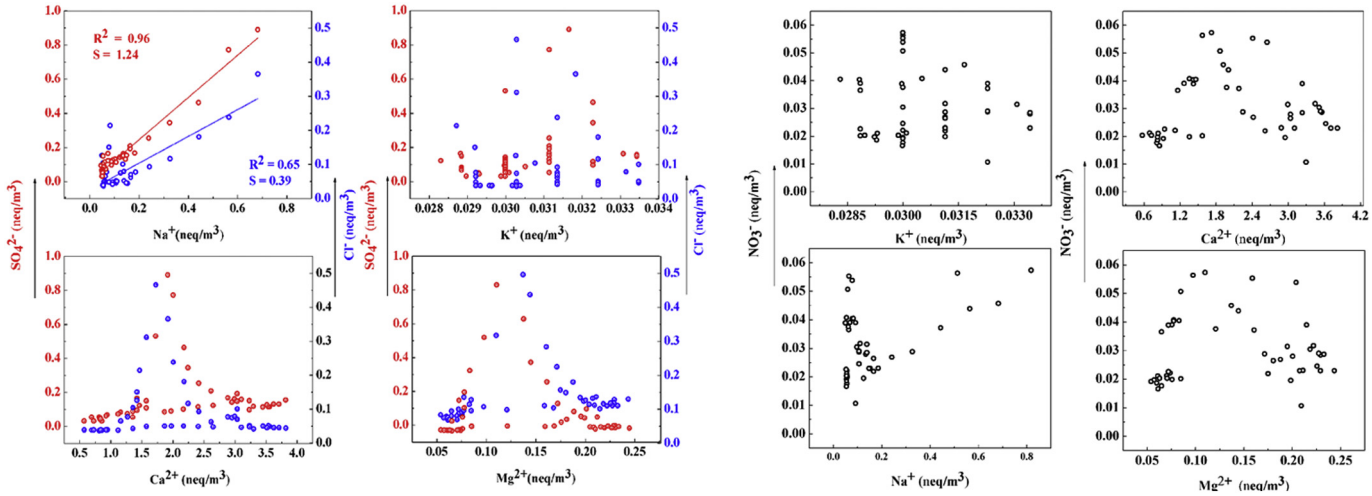

Fig. 6. Linear regression between cations (Ca^{2+}, Mg^{2+}, K^{+}, and Na^{+}) and anions (SO_4^{2-} (red circle), Cl^{-} (blue circle), and NO_3^{-} (black circle)) for measurements in the dust event.

SO_2 (Ohta and Okita, 1990). In our case, the mean value of SOR averaged over the dust event were 0.64, which was 1.33 times than that in the non-dust period (0.48), indicating that the secondary transformation played an appreciable role in the dust event.

The ratio of SO_4^{2-} to SO_2 is used to characterize the formation route and source of SO_4^{2-} (Sievering et al., 1991). The average value of $[SO_4^{2-}]/[SO_2]$ was 2.7 in the dust event, about 2.31 times greater than that in the non-dust period (1.17). Under the same temperature in the non-dust period and dust event, we could deduce that except for local gas phase oxidation of SO_2, the long-range transport exerted a large impact on the air quality in Lanzhou in the dust event.

3.5. HYSPLIT analysis

To interpret the origins of water-soluble ions during the dust event, the 48-hour backward trajectory analysis started at 500 m from Lanzhou was carried out by using the HYSPLIT model. Results clearly revealed the air parcels extended from different origins, as illustrated in Fig. 8. The air parcel #1 arriving at the sampling site was originated from the border of Xinjiang Province and Gansu Province, passing through Qinghai Province where there are many salt lakes. This air parcel then swirled in the urban are of Lanzhou and finally arrived in the city. Hence, this trajectory characterized high loadings of SO_4^{2-}, Cl^{-},

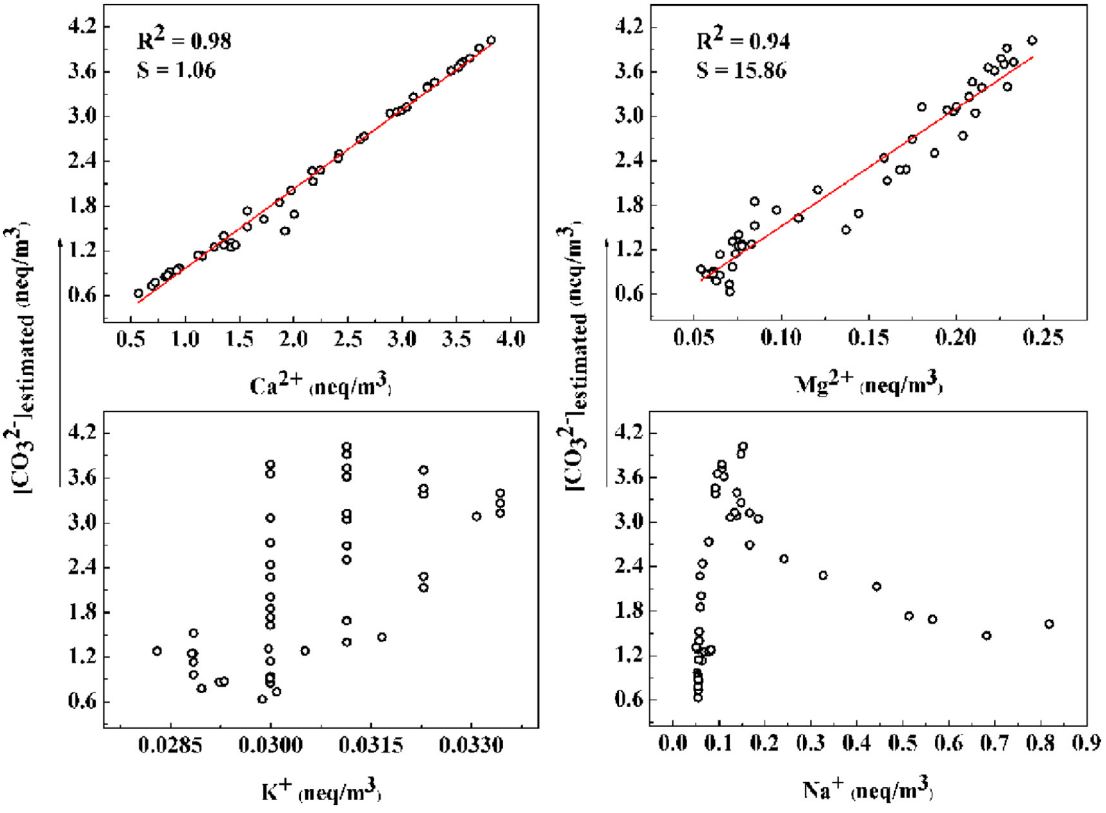

Fig. 7. Linear regression between measured cations (Ca^{2+}, Mg^{2+}, K^{+}, and Na^{+}) and estimated CO_3^{2-} in the dust event.

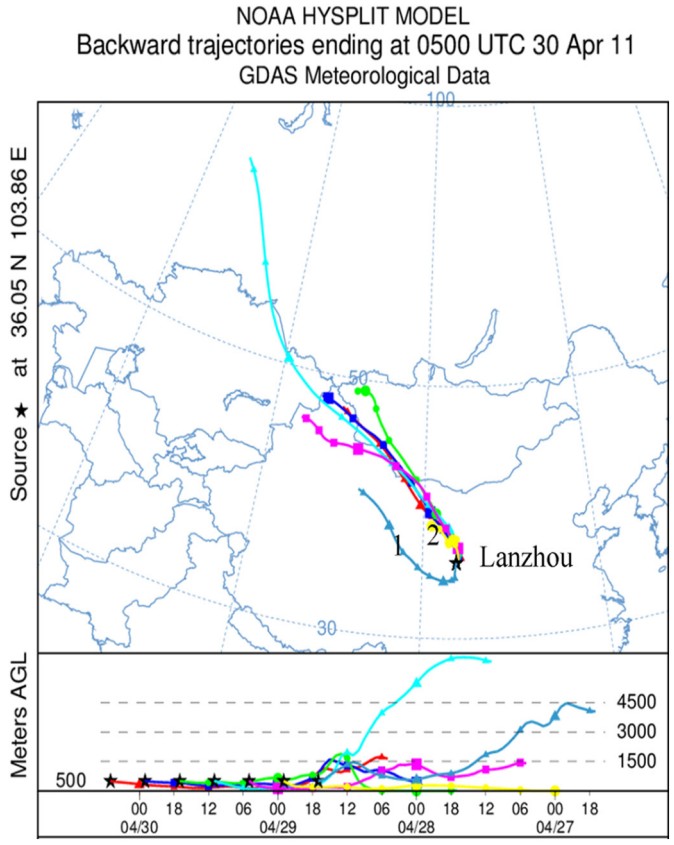

Fig. 8. NOAA HYSPLIT Model result with GDAS meteorological data. 72-h backward trajectories are ended at 05:00 UTC, Apr 30th.

and Na^+. The rest of air parcels remotely traveled through the Desert such as Gurbantunggut Desert from the northwest of Xinjiang and the Gobi Deserts in southern Mongolia, successively arrived the sampling site, forming another peak characterized by abundant Mg^{2+} and Ca^{2+}. When the dust occurred, the origins and compositions of aerosols were different before and after the cold front associated with the movement of cyclones. Particles in the prefrontal air normally were originated from local or regional sources and moved from the south or southwest to the north or northeast. Therefore, the prefrontal air masses usually carried a large number of anthropogenic pollutants (Li et al., 2012). Particles in the postfrontal air were originated from the remote sources in the north or northwest of Lanzhou (Wang et al., 2006). Since the prefrontal and postfrontal air masses had different originations held different components of pollutants, and arrived at the sampling point at different time. Such different time interval before and after the cold front further demonstrated the different origins of the different air parcels.

In the non-dust period, the backward trajectory cluster and corresponding cluster statistics of water-soluble ions were depicted in Fig. 9. According to their origins and paths, all the trajectories could be classified into 5 categories: (1) southern airflow, (2) northern air masses, (3) the northwest parcel associated with the long-range atmospheric transport, (4) rotary air masses from north, and (5) northwest airflow. From Fig. 9, it can be seen that, in addition to cluster 1, which originated from the south and accounted for 9.8% of the total number of trajectories, almost all trajectories were originated from the north or northwest of the sampling site. The northwest parcel associated with long-range transport (cluster 3) was the most frequent and accounted for 36.1% of total trajectories, whereas the north air masses from Mongolia also played an important role in the air masses arriving at Lanzhou as it contributed 26.2% to the total trajectories (cluster 2).

The highest concentrations of NO_3^-, SO_4^{2-}, and Ca^{2+} were observed in the cluster 3, indicating that secondary ions in PM_{10} were readily formed during the long-range transport from their upwind sources. Among them, Ca^{2+} concentration tends to be enriched because of the vast region covered by Gobi-desert (Karaca and Camci, 2010). The air masses in Cluster 3 were essentially originated from the Taklimakan Desert and Kumtag Desert in Xinjiang Province, traveled through Qinghai, and then arrived at the sampling site. Many salt lakes in Qinghai Province also contributed to Cl^- abundance.

Much higher concentrations of Ca^{2+}, SO_4^{2-}, and NO_3^- were connected with air masses from north or northwest including cluster 2,

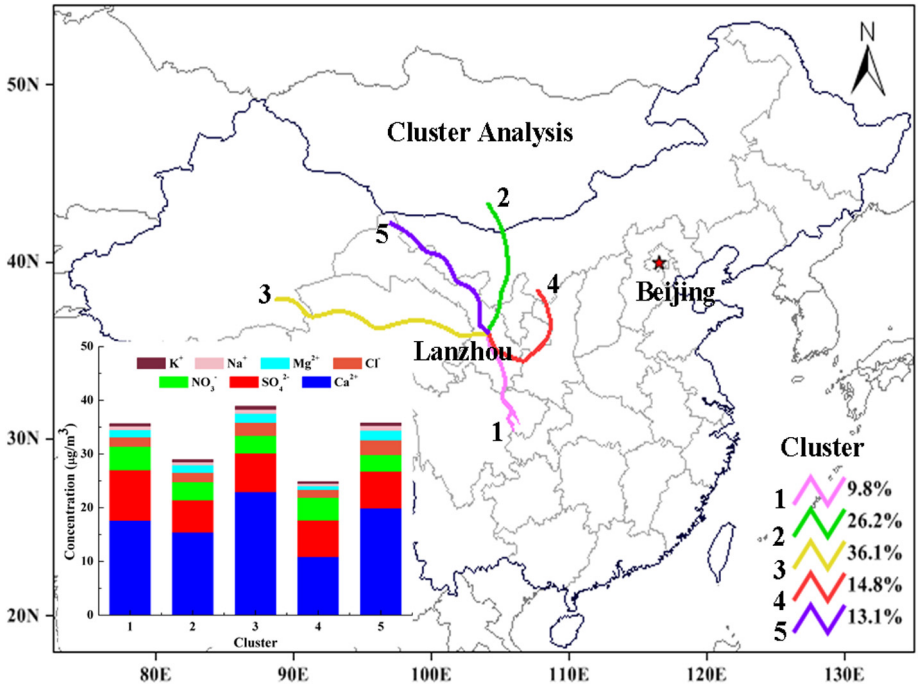

Fig. 9. Backward trajectory cluster and the corresponding cluster statistics (inserted figure) in the non-dust period.

cluster 4, and cluster 5. The air masses in cluster 2 originated from Mongolia, passing over Inner Mongolia before arriving at Lanzhou. The air masses in cluster 4 contained the lowest Ca^{2+} originated from the south of Inner Mongolia, moved southerly and finally turned westerly to Lanzhou. The air masses in cluster 5 were mostly originated from the northwest of Lanzhou, and partially traveled though Inner Mongolia with the almost number of trajectories but held larger amount of Ca^{2+} and SO_4^{2-} than that in cluster 4. Lower concentrations of NO_3^-, SO_4^{2-}, and Ca^{2+} were identified in cluster 1 with the air masses mostly from Sichuan Province, which moved northwesterly to Lanzhou via industrial zones with high emissions of primary pollutants. This pathway brought larger abundant SO_4^{2-} as compared with other trajectories (Chang et al., 2009).

3.6. Source apportionment by PMF

PMF analysis was used to assess the contribution of the different sources to the water-soluble ions. The source profiles and contributions gained from PMF 5.0 in the non-dust period and dust event were displayed in Figs. 10 and 11, respectively. In the non-dust period, three factors were extracted by the model. The first factor showed high levels of NH_4^+, NO_3^-, and SO_4^{2-}, characterizing the secondary aerosols (Gao et al., 2011). Hence, this factor could explain the secondary sources and contributed 33.98% to the mass concentration of water-soluble ions. The second factor correlated strongly with K^+, Cl^-, and relatively strongly with Na^+. K^+ is a tracer of biomass burning which includes domestic burning of firewood and agricultural residues and Cl^- might be emitted from coal combustion (Chow et al., 2004; Singh and Sharma, 2012). This factor represents a combination of coal and biomass burning. Mg^{2+} and Ca^{2+} were identified as the third factor which made a dominate contribution 58.09% to the water-soluble ions. This factor characterizes the impact of local construction materials and re-suspended dust (Nicolás et al., 2009). As discussed in Section 3.5, the air quality in Lanzhou also associated largely with the air parcels from Desert regions over the non-dust period, crustal materials from these deserts could be also linked with the factor 3 in the context of the water-soluble ions.

In the dust event, four sources were identified. The first one was attributed to the dust source via the long-range transport from the Gurbantunggut Desert, which contributed 8.92% to the water-soluble ions. The second factor was dominated by high loadings of K^+ largely due to biomass burning, this factor only explained 0.8% of the loading of total water-soluble ions. The third factor featured large amount of Cl^-, Na^+, and SO_4^{2-}. As discussed in Section 3.5, we inferred that this factor represented the aerosols transported to Lanzhou over long distance from salt lakes. This factor contributed as much as 29.68% to the loading of water soluble ions. The forth factor was represented by NO_3^- which was emitted from motor vehicle, contributed 2.51% to the water-soluble ions.

3.7. The potential source-area analysis

Fig. 12 shows the results of CWT analysis for water-soluble ions in PM_{10}, respectively. As NH_4NO_3 is a semi-volatile species, its concentration is strongly influenced by the air temperature and relative humidity during its atmospheric transport (Mozurkewich, 1993), the potential source-area of NH_4^+ was not analyzed in the present study. Serval features can be identified in Fig. 12: (1) NO_3^-, Cl^-, and K^+ basically had the same spatial patterns with the darker color near the receptor region (Lanzhou), indicating that these ions were local pollutants. (2) Na^+, Mg^{2+}, and Ca^{2+} show similar spatial distributions with two main potential regions from different sources. The one was identified in the areas around or in Lanzhou which might be caused by floating dust induced by construction or re-suspended agricultural field dust. The other one was identified on the border region of Xinjiang, Qinghai, and Gansu. (3) The potential sources of SO_4^{2-} were adjacent to Lanzhou and its spatial pattern was nicely consistent with its precursor SO_2 (Fig. S5). In general, the potential sources near the Lanzhou contributed the most to the secondary ions and potential sources located in the border of Xinjiang, Qinghai and Gansu contributed most to the mineral ions.

4. Conclusion

In this study, trace gases and water-soluble ions were measured and compared in the springtime, 2011, the season with frequently occurring dust storms in Lanzhou. The mean concentrations of water-soluble ions in the dust event were 0.55–4.29 times higher than that in the non-dust period, trace gases in the dust event all decreased except HCl. In the non-dust period, diurnal variations of SO_4^{2-}, NO_3^-, and their gaseous precursors exhibited a similar pattern with the maximum concentrations at 09:00–10:00 LT, and the minimum concentrations at 18:00–19:00 LT. NH_4^+ shows the unimodal temporal pattern with one peak at 09:00 LT, and the other occurred at 19:00 LT. NH_3 shows a bimodal pattern whereas, HCl and Cl^- illustrated an opposite diurnal pattern. In the dust event, Except for HNO_3 and NO_3^-, temporal profiles of HCl and Cl^-, SO_2 and SO_4^{2-} all presented similar change trend with unimodal pattern, and dust ions (Ca^{2+} and Mg^{2+}) lagged 13 h to Na^+, SO_4^{2-}, and Cl^-. Equivalent ratio analysis revealed that the chemical composition of dust particles unaltered after the long-range transport.

The mean mass ratios of NO_3^- to SO_4^{2-} revealed the importance of stationary sources than mobile sources in both dust event and non-dust period. As the $[NO_3^-]/[SO_4^{2-}]$ in the dust period was a factor of 1.8 lower than that in the non-dust period, indicating higher SO_4^{2-} in the dust event. The SOR and $[SO_4^{2-}]/[SO_2]$ ratios manifested that the long-

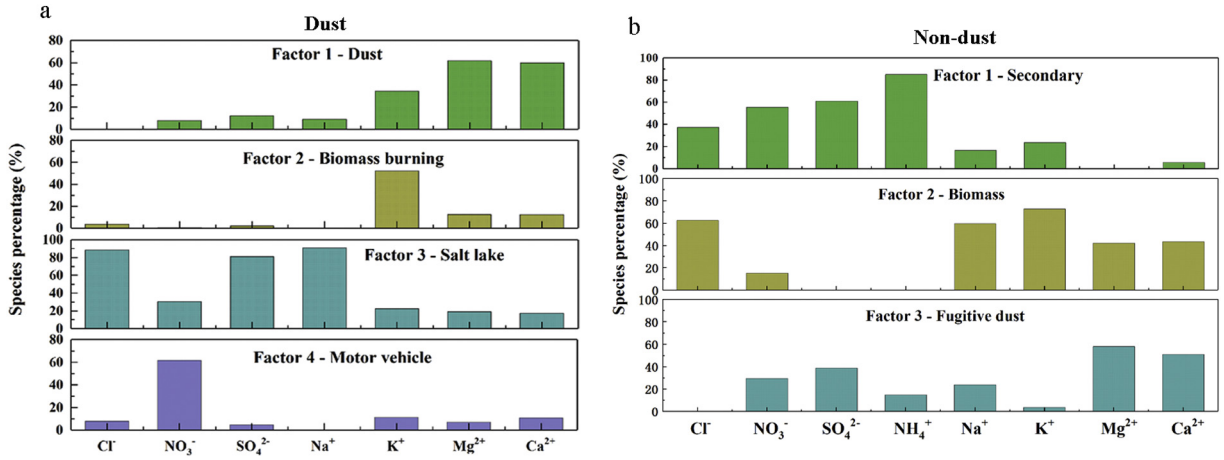

Fig. 10. Factor profiles from execution of PMF 5.0 in the dust event (a) and non-dust period (b).

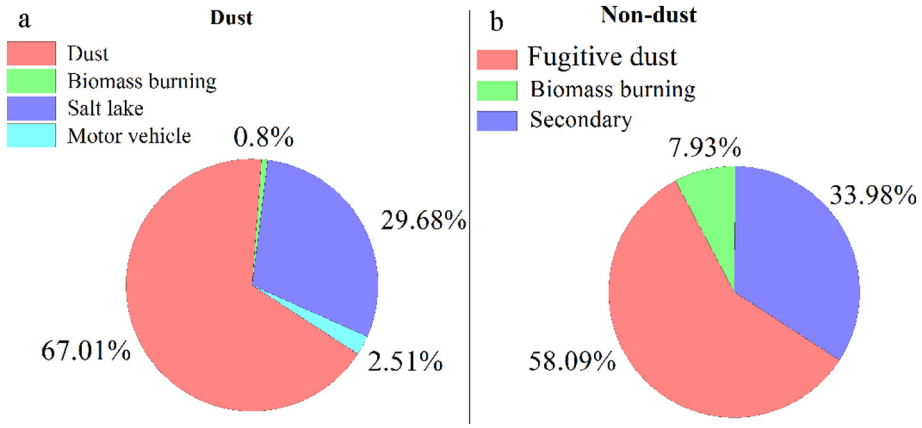

Fig. 11. Contributions of different sources to water-soluble ions in the dust event (a) and non-dust period (b).

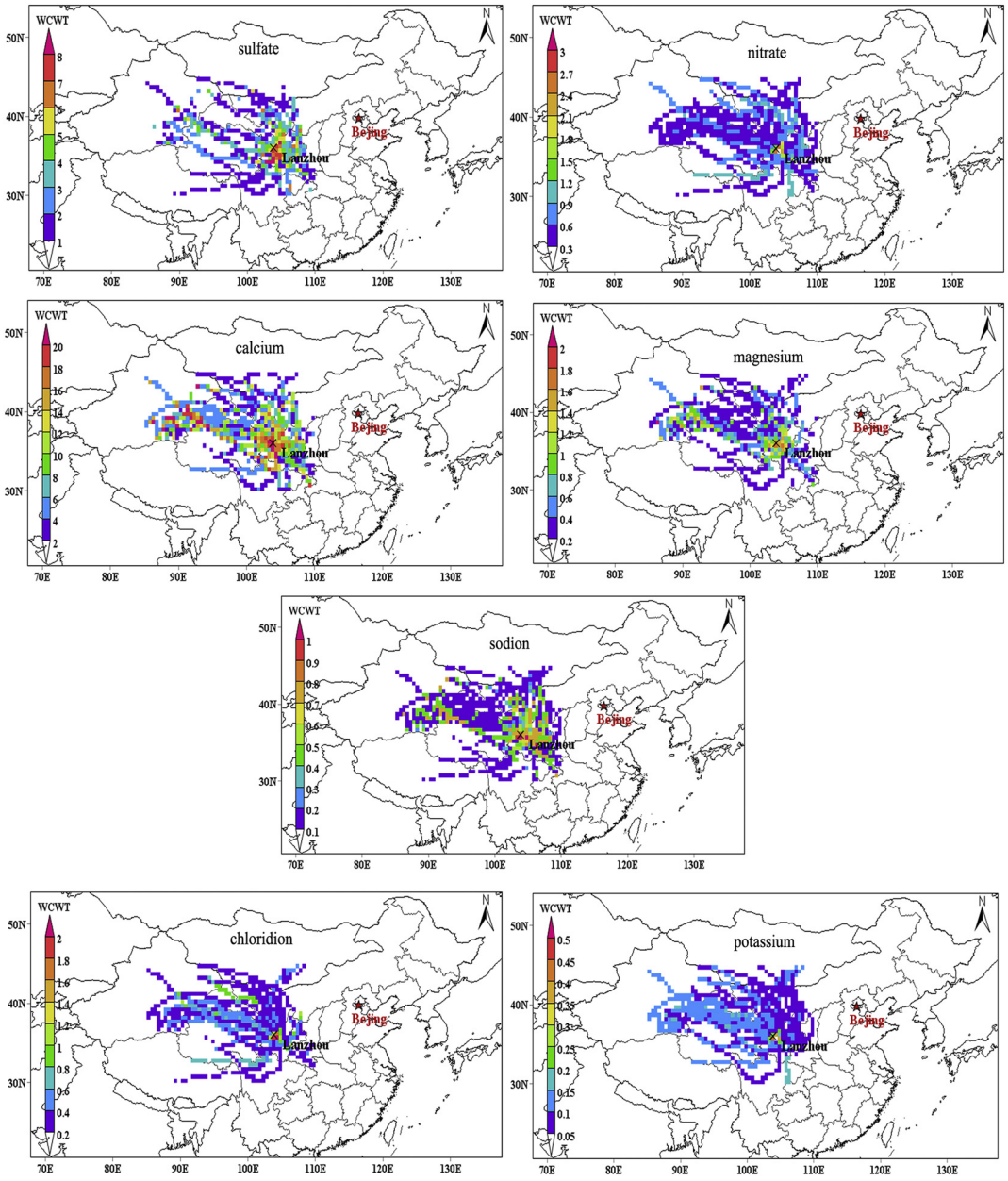

Fig. 12. The WCWT maps for measured water-soluble ions in the whole campaign (The color corresponds to the probability for the emission areas as origin of the measured water-soluble ions in Lanzhou (black fork), the darker the color, the stronger the potential source is).

range transport of SO_4^{2-} accounted for a much larger proportion of sulfate than gas phase oxidation of SO_2. PMF results indicated that fugitive dust contributed significantly to water soluble ions and PM contamination in Lanzhou in spring. Cl^-, Na^+, and SO_4^{2-} from salt-lakes exerted a more significant impact than crustal ions from Gurbantunggut Desert via the long-range transport in the dust event.

The CWT results indicated that the potential sources of NO_3^-, Cl^-, and K^+ were local sources in and near Lanzhou. The potential sources of Na^+, Mg^{2+}, and Ca^{2+} could be traced back to the areas in the vicinity of Lanzhou and the border region of Xinjiang, Qinghai and Gansu. The potential sources of SO_4^{2-} were, however, local which is proximate to Lanzhou.

Acknowledgements

The authors gratefully acknowledge the financial support provided by the National Key R&D Program of China under contract 2016YFC0206201, the Strategic Priority Research Program of the Chinese Academy of Sciences (class A) (XDA2006020103), and the SKLCS founding (SKLCS-ZZ-2018).

Appendix A. Supplementary data

Supplementary data to this article can be found online at https://doi.org/10.1016/j.scitotenv.2018.09.382.

References

Arimoto, R., Duce, R.A., Savoie, D.L., Prospero, J.M., Talbot, R., Cullen, J.D., Tomza, U., Lewis, N.F., Ray, B.J., 1996. Relationships among aerosol constituents from Asia and the North Pacific during PEM-West A. J. Geophys. Res. Atmos. 101, 2011–2023. https://doi.org/10.1029/95JD01071.

Bari, A., Ferraro, V., Wilson, L.R., Luttinger, D., Husain, L., 2003. Measurements of gaseous HONO, HNO_3,SO_2, HCl, NH_3, particulate sulfate and $PM_{2.5}$ in New York, NY. Atmos. Environ. 37, 2825–2835. https://doi.org/10.1134/S0020441207060061.

Bates, T.S., Quinn, P.K., Coffman, D.J., Covert, D.S., Miller, T.L., Johnson, J.E., Carmichael, G.R., Uno, I., Guazzotti, S.A., Sodeman, D.A., 2004. Marine boundary layer dust and pollutant transport associated with the passage of a frontal system over eastern Asia. J. Geophys. Res. Atmos. 109, 3644–3657. https://doi.org/10.1029/2003JD004094.

Battye, W., Aneja, V.P., Roelle, P.A., 2003. Evaluation and improvement of ammonia emissions inventories. Atmos. Environ. 37, 3873–3883. https://doi.org/10.1016/S1352-2310(03)00343-1.

Behera, S., Betha, R., Balasubramanian, R., 2013. Insights into chemical coupling among acidic gases, ammonia and secondary inorganic aerosols. Aerosol Air Qual. Res. 13, 1282–1296. https://doi.org/10.4209/aaqr.2012.11.0328.

Biswas, K.F., Ghauri, B.M., Husain, L., 2008. Gaseous and aerosol pollutants during fog and clear episodes in South Asian urban atmosphere. Atmos. Environ. 42, 7775–7785. https://doi.org/10.1016/j.atmosenv.2008.04.056.

Cao, J.J., Xu, H., Xu, Q., Chen, B., Kan, H., 2012a. Fine particulate matter constituents and cardiopulmonary mortality in a heavily polluted Chinese city. Environ. Health Perspect. 120, 373–378. https://doi.org/10.1289/ehp.1103671.

Cao, J.J., Zhu, C.S., Tie, X.X., Geng, F.H., Xu, H.M., Ho, S.S.H., Wang, G.H., Han, Y.M., Ho, K.F., 2012b. Characteristics and sources of carbonaceous aerosols from Shanghai, China. Atmos. Chem. Phys. 12, 803–817. https://doi.org/10.5194/acpd-12-16811-2012.

Chang, D., Song, Y., Liu, B., 2009. Visibility trends in six megacities in China 1973–2007. Atmos. Res. 94, 161–167. https://doi.org/10.1016/j.atmosres.2009.05.006.

Cheng, M.D., Hopke, P.K., Zeng, Y., 1993. A receptor-oriented methodology for determining source regions of particulate sulfate observed at Dorset, Ontario. J. Geophys. Res. Atmos. 98, 16839–16849. https://doi.org/10.1029/92JD02622.

Choi, I.J., Kim, S.W., Kim, J., Yoon, S.C., Kim, M.H., Sugimoto, N., Kondo, Y., Miyazaki, Y., Moon, K.J., Han, J.S., 2008. Characteristics of the transport and vertical structure of aerosols during ABC-EAREX2005. Atmos. Environ. 42, 8513–8523. https://doi.org/10.1016/j.atmosenv.2008.05.060.

Chow, J.C., Watson, J.G., Kuhns, H., Etyemezian, V., Lowenthal, D.H., Crow, D., Kohl, S.D., Engelbrecht, J.P., Green, M.C., 2004. Source profiles for industrial, mobile, and area sources in the Big Bend Regional Aerosol Visibility and Observational study. Chemosphere 54, 185–208. https://doi.org/10.1016/j.chemosphere.2003.07.004.

Dao, X., Wang, Z., Lv, Y., Teng, E., Zhang, L., Wang, C., 2014. Chemical characteristics of water-soluble ions in particulate matter in three metropolitan areas in the North China Plain. PLoS One 9, 0113831. https://doi.org/10.1371/journal.pone.0113831.

Derwent, R., Witham, C., Redington, A., Jenkin, M., Stedman, J., Yardley, R., Hayman, G., 2009. Particulate matter at a rural location in southern England during 2006: model sensitivities to precursor emissions. Atmos. Environ. 43, 689–696. https://doi.org/10.1016/j.atmosenv.2008.09.077.

Dibb, J.E., Talbot, R.W., Whitlow, S.I., Shipham, M.C., Winterle, J., McConnell, J., Bales, R., 1996. Biomass burning signatures in the atmosphere and snow at Summit, Greenland: an event on 5 August 1994. Atmos. Environ. 30, 553–561. https://doi.org/10.1016/1352-2310(95)00328-2.

Ding, X., Kong, L., Du, C., Zhanzakova, A., Lin, W., Fu, H., Chen, J., Xin, Y., Cheng, T., 2017. Long-range and regional transported size-resolved atmospheric aerosols during summertime in urban Shanghai. Sci. Total Environ. 583, 334–343. https://doi.org/10.1016/j.scitotenv.2017.01.073.

Draxler, R.R., Hess, G.D., 1998. An overview of the hysplit-4 modeling system for trajectories. Aust. Meteorol. Mag. 47, 295–308.

Du, H., Kong, L., Cheng, T., Chen, J., Du, J., Li, L., Xia, X., Leng, C., Huang, G., 2011. Insights into summertime haze pollution events over Shanghai based on online water-soluble ionic composition of aerosols. Atmos. Environ. 45, 5131–5137. https://doi.org/10.1016/j.atmosenv.2011.06.027.

Duan, F., Liu, X., Yu, T., Cachier, H., 2004. Identification and estimate of biomass burning contribution to the urban aerosol organic carbon concentrations in Beijing. Atmos. Environ. 38, 1275–1282. https://doi.org/10.1016/j.atmosenv.2003.11.037.

Eldering, A.M., Solomon, P.A., Salmon, L.G., Fall, T., Cass, G.R., 1991. Hydrochloric acid: a regional perspective on concentrations and formation in the atmosphere of Southern California. Atmos. Environ. 25, 2091–2102. https://doi.org/10.1016/0960-1686(91)90086-M.

Erduran, M.S., Tuncel, S.G., 2001. Gaseous and particulate air pollutants in the Northeastern Mediterranean Coast. Sci. Total Environ. 281, 205–215. https://doi.org/10.1016/S0048-9697(01)00847-6.

Fang, X., Zou, B., Liu, X., Sternberg, T., Zhai, L., 2016. Satellite-based ground $PM_{2.5}$ estimation using timely structure adaptive modeling. Remote Sens. Environ. 186, 152–163. https://doi.org/10.1016/j.rse.2016.08.027.

Finlayson-Pitts, B.J., 2009. Reactions at surfaces in the atmosphere: integration of experiments and theory as necessary (but not necessarily sufficient) for predicting the physical chemistry of aerosols. Phys. Chem. Chem. Phys. 11, 7760–7779. https://doi.org/10.1039/B906540G.

Formenti, P., Schütz, L., Balkanski, Y., Desboeufs, K., 2010. Recent progress in understanding physical and chemical properties of African and Asian mineral dust. Atmos. Chem. Phys. Discuss. 10, 8231–8256. https://doi.org/10.5194/acpd-10-31187-2010.

Galindo, N., Gil-Moltó, J., Varea, M., Chofre, C., Yubero, E., 2013. Seasonal and interannual trends in PM levels and associated inorganic ions in southeastern Spain. Microchem. J. 110, 81–88. https://doi.org/10.1016/j.microc.2013.02.009.

Gao, X., Yang, L., Cheng, S., Gao, R., Zhou, Y., Xue, L., Shou, Y., Wang, J., Wang, X., Nie, W., 2011. Semi-continuous measurement of water-soluble ions in $PM_{2.5}$ in Jinan, China: temporal variations and source apportionments. Atmos. Environ. 45, 6048–6056. https://doi.org/10.1016/j.atmosenv.2011.07.041.

Han, B., 2013. The Exhaust Emission Characteristics of Motor Vehicle in Lanzhou. (Master thesis in Chinese). Lanzhou Jiaotong University, Lanzhou.

Han, J., 2014. Chemical characterizations of PM_{10} profiles for major emission sources in Xining, Northwestern China. Aerosol Air Qual. Res. 14, 1017–1027. https://doi.org/10.4209/aaqr.2013.01.0027.

Harris, J.M., Kahl, J.D., 1990. A descriptive atmospheric transport climatology for the Mauna Loa Observatory, using clustered trajectories. J. Geophys. Res. Atmos. 95, 13651–13667. https://doi.org/10.1029/JD095iD09p13651.

Hatakeyama, S., Takami, A., Sakamaki, F., Mukai, H., Sugimoto, N., Shimizu, A., Bandow, H., 2004. Aerial measurement of air pollutants and aerosols during 20–22 March 2001 over the East China Sea. J. Geophys. Res. Atmos. 109, D13304. https://doi.org/10.1029/2003JD004271.

Hear, M.R., Kumar, P., Harrison, R.M., 2012. Particles, air quality, policy and health. Chem. Soc. Rev. 41, 6606–6630. https://doi.org/10.1039/c2cs35076a.

Heland, J., Kleefmann, J., Kurtenbach, R., Wiesen, P., 2001. A new instrument to measure gaseous nitrous acid (HONO) in the atmosphere. Environ. Sci. Technol. 35, 3207–3212. https://doi.org/10.1021/es000303t.

Hesterberg, R., Blatter, A., Fahrni, M., Rosset, M., Neftel, A., Eugster, W., Wanner, H., 1996. Deposition of nitrogen-containing compounds to an extensively managed grassland in central Switzerland. Environ. Pollut. 91, 21–34. https://doi.org/10.1016/0269-7491(95)00036-Q.

Hopke, P.K., Gao, N., Cheng, M.D., 1993. Combining chemical and meteorological data to infer source areas of airborne pollutants. Chemom. Intell. Lab. Syst. 19, 187–199. https://doi.org/10.1016/0169-7439(93)80103-O.

Hsu, Y.K., Holsen, T.M., Hopke, P.K., 2003. Comparison of hybrid receptor models to locate PCB sources in Chicago. Atmos. Environ. 37, 545–562. https://doi.org/10.1016/S1352-2310(02)00886-5.

Hu, J., Ying, Q., Wang, Y., Zhang, H., 2015. Characterizing multi-pollutant air pollution in China: comparison of three air quality indices. Environ. Int. 84, 17–25. https://doi.org/10.1016/j.envint.2015.06.014.

Huang, K., Zhuang, G., Li, J., Wang, Q., Sun, Y., Lin, Y., Fu, J.S., 2010a. Mixing Asian dust with pollution aerosol and the transformation of aerosol components during the dust storm over China in spring 2007. J. Geophys. Res. Atmos. 115, D00K13. https://doi.org/10.1029/2009JD013145.

Huang, K., Zhuang, G., Lin, Y., Li, J., Sun, Y., Zhang, W., Fu, J.S., 2010b. Relation between optical and chemical properties of dust aerosol over Beijing, China. J. Geophys. Res. Atmos. 115, D00K16. https://doi.org/10.1029/2009JD013212.

Jacob, D.J., 1999. Introduction to Atmospheric Chemistry. Princeton University Press https://www.jstor.org/stable/j.ctt7t8hg.

Jiang, Y., Zhang, Y., 2011. The zoology distribution and characteristics of the saline soil in Shengyang area. Soil Bull. 32 (z1), 124–127. https://doi.org/10.19336/j.cnki.trtb.2001.s1.031 (in Chinese).

Karaca, F., Camci, F., 2010. Distant source contributions to PM_{10} profile evaluated by SOM based cluster analysis of air mass trajectory sets. Atmos. Environ. 44, 892–899. https://doi.org/10.1016/j.atmosenv.2009.12.006.

Keeler, G.J., 1987. A Hybrid Approach for Source Apportionment of Atmospheric Pollutants in the Northeastern United States.

Kim, K.H., Kabir, E., Kabir, S., 2015. A review on the human health impact of airborne particulate matter. Environ. Int. 74, 136–143. https://doi.org/10.1016/j.envint.2014.10.005.
Kirkby, J., Curtius, J., Almeida, J., Dunne, E., Duplissy, J., Ehrhart, S., Franchin, A., Gagné, S., Ickes, L., Kürten, A., 2011. Role of sulphuric acid, ammonia and galactic cosmic rays in atmospheric aerosol nucleation. Nature 476, 429–433. https://doi.org/10.1038/nature10343.
Kleffmann, J., Kurtenbach, R., Lörzer, J., Wiesen, P., Kalthoff, N., Vogel, B., Vogel, H., 2003. Measured and simulated vertical profiles of nitrous acid-part I: field measurements. Atmos. Environ. 37, 2949–2955. https://doi.org/10.1016/S1352-2310(03)00242-5.
Koçak, M., Mihalopoulos, N., Tutsak, E., Theodosi, C., Zarmpas, P., Kalegeri, P., 2015. PM_{10} and $PM_{2.5}$ composition over the Central Black Sea: origin and seasonal variability. Environ. Sci. Pollut. Res. Int. 22, 18076–18092. https://doi.org/10.1007/s11356-015-4928-2.
Kulmala, M., Pirjola, L., Mäkelä, J.M., O'Dowd, C.D., 2000. Stable sulfate clusters as a source of new atmospheric particles. Nature 534, 66–69. https://doi.org/10.1063/1.1362003.
Kulshrestha, U.C., Raman, R.S., Kulshrestha, M.J., Rao, T.N., Hazarika, P.J., 2009. Secondary aerosol formation and identification of regional source locations by PSCF analysis in the Indo-Gangetic region of India. J. Atmos. Chem. 63, 33–47. https://doi.org/10.1007/s10874-010-9156-z.
Kunwar, B., Torii, K., Zhu, C., Fu, P., Kawamura, K., 2016. Springtime variations of organic and inorganic constituents insubmicron aerosols ($PM_{1.0}$) from Cape Hedo, Okinawa. Atmos. Environ. 130, 84–94. https://doi.org/10.1016/j.atmosenv.2015.09.002.
Lee, Y.N., Weber, R., Ma, Y., Orsini, D., Maxwell-Meier, K., Blake, D., Meinardi, S., Sachse, G., Harward, C., Chen, T.Y., 2003a. Airborne measurement of inorganic ionic components of fine aerosol particles using the particle-into-liquid sampler coupled to ion chromatography technique during ACE-Asia and TRACE-P. J. Geophys. Res. Atmos. 108, 2932–2938. https://doi.org/10.1029/2002JD003265.
Lee, P.K, Brook, J.R, Dabek-Zlotorzynska, E., Mabury, S.A., 2003b. Identification of the major sources contributing to PM2.5 observed in Toronto.[J]. Environ. Sci. Technol. 37, 4831–4840. https://doi.org/10.1021/es026473i.
Li, G., Chen, J., Chen, Y., Yang, J., Ji, J., Liu, L., 2007. Dolomite as a tracer for the source regions of Asian dust. J. Geophys. Res. 112, D17201. https://doi.org/10.1029/2007JD008676.
Li, M., Huang, X., Zhu, L., Li, J., Song, Y., Cai, X., Xie, S., 2012. Analysis of the transport pathways and potential sources of PM_{10} in Shanghai based on three methods. Sci. Total Environ. 414, 525–534. https://doi.org/10.1016/j.scitotenv.2011.10.054.
Liang, C.S., Duan, F.K., He, K.B., Ma, Y.L., 2016. Review on recent progress in observations, source identifications and countermeasures of $PM_{2.5}$. Environ. Int. 86, 150–170. https://doi.org/10.1016/j.envint.2015.10.016.
Liang, T., Tong, Y., Liu, X., Xu, W., Luo, X., Christie, P., 2016. High nitrogen deposition in an agricultural ecosystem of Shanxi, China. Environ. Sci. Pollut. Res. Int. 23, 13210–13221. https://doi.org/10.1007/s11356-016-6374-1.
Lin, J.J., 2002. Characterization of water-soluble ion species in urban ambient particles. Environ. Int. 28, 55–61. https://doi.org/10.1016/S0160-4120(02)00004-1.
Lin, Y.C., Cheng, M.T., Ting, W.Y., Yeh, C.R., 2006. Characteristics of gaseous HNO, HNO_3, NH_3 and particulate ammonium nitrate in an urban city of Central Taiwan. Atmos. Environ. 40, 4725–4733. https://doi.org/10.1016/j.atmosenv.2006.04.037.
Liu, X., Van Espen, P., Adams, F., Cafmeyer, J., Maenhaut, W., 2000. Biomass burning in southern Africa: individual particle characterization of atmospheric aerosols and savanna fire samples. J. Atmos. Chem. 36, 135–155. https://doi.org/10.1023/A:1006387031927.
Ma, Y., Weber, R.J., Lee, Y.N., Orsini, D.A., Maxwell-Meier, K., Thornton, D.C., Bandy, A.R., Clarke, A.D., Blake, D.R., Sachse, G.W., 2003. Characteristics and influence of biosmoke on the fine-particle ionic composition measured in Asian outflow during the Transport and Chemical Evolution Over the Pacific (TRACE-P) experiment. J. Geophys. Res. Atmos. 108, 1919–1964. https://doi.org/10.1029/2002JD003128.
Maher, B.A., Mutch, T.J., Cunningham, D., 2009. Magnetic and geochemical characteristics of Gobi Desert surface sediments: implications for provenance of the Chinese Loess Plateau. Geology 37, 279–282. https://doi.org/10.1130/G25293A.1.
Makkonen, U., 2014. Semi-continuous gas and inorganic aerosol measurements at a boreal forest site: seasonal and diurnal cycles of NH_3, HONO and HNO_3. Boreal Environ. Res. 19, 311–328.
Matsumoto, K., Uyama, Y., Hayano, T., Tanimoto, H., Uno, I., Uematsu, M., 2003. Chemical properties and outflow patterns of anthropogenic and dust particles on Rishiri Island during the Asian Pacific Regional Aerosol Characterization Experiment (ACE-Asia). J. Geophys. Res. Atmos. 108, 8666. https://doi.org/10.1029/2003JD003426.
Maxwell-Meier, K., Weber, R., Song, C., Orsini, D., Ma, Y., Carmichael, G.R., Streets, D.G., 2004. Inorganic composition of fine particles in mixed mineral dust–pollution plumes observed from airborne measurements during ACE-Asia. J. Geophys. Res. Atmos. 109, D19S07. https://doi.org/10.1029/2003JD004464.
Mozurkewich, M., 1993. The dissociation constant of ammonium nitrate and its dependence on temperature, relative humidity and particle size. Atmos. Environ. 27, 261–270. https://doi.org/10.1016/0960-1686(93)90356-4.
Nava, S., Becherini, F., Bernardi, A., Bonazza, A., Chiari, M., Garcã-A-Orellana, I., Lucarelli, F., Ludwig, N., Migliori, A., Sabbioni, C., 2016. An integrated approach to assess air pollution threats to cultural heritage in a semi-confined environment: the case study of Michelozzo's Courtyard in Florence (Italy). Nutr. Cycl. Agroecosyst. 106, 47–59. https://doi.org/10.1016/j.scitotenv.2009.07.030.
Ndour, M., D'Anna, B., George, C., Ka, O., Balkanski, Y., Kleffmann, J., Stemmler, K., Ammann, M., 2008. Photoenhanced uptake of NO_2 on mineral dust: Laboratory experiments and model simulations. Geophys. Res. Lett. 35 (iii–v). https://doi.org/10.1029/2007GL032006.
Nicolás, J.F., Galindo, N., Yubero, E., Pastor, C., Esclapez, R., Crespo, J., 2009. Aerosol inorganic ions in a semiarid region on the southeastern Spanish Mediterranean coast. Water Air Soil Pollut. 201, 149–159. https://doi.org/10.1007/s11270-008-9934-2.
Norris, G., 2014. EPA Positive Matrix Factorization (PMF) 5.0 Fundamentals & User Guide. U.S. Environmental Protection Agency.
Ocskay, R., Salma, I., Wang, W., Maenhaut, W., 2006. Characterization and diurnal variation of size-resolved inorganic water-soluble ions at a rural background site. J. Environ. Monit. 8, 300–306. https://doi.org/10.1039/b513915e.
Ohta, S., Okita, T., 1990. A chemical characterization of atmospheric aerosol in Sapporo. Atmos. Environ. A. Gen. Top. 24, 815–822. https://doi.org/10.1016/0960-1686(90)90282-R.
Osada, K., Kido, M., Nishita, C., Matsunaga, K., Iwasaka, Y., Nagatani, M., Nakada, H., 2002. Changes in ionic constituents of free tropospheric aerosol particles obtained at Mt. Norikura (a.s.l.), central Japan, during the Shurin period in 2000. Atmos. Environ. 36, 5469–5477. https://doi.org/10.1016/S1352-2310(02)00663-5.
Paatero, P., Tapper, U., 1994. Positive matrix factorization: A non-negative factor model with optimal utilization of error estimates of data values. Environmetrics 5, 111–126. https://doi.org/10.1002/env.3170050203.
Paatero, P., 1997. A weighted non-negative least squares algorithm for three-way 'PARAFAC' factor analysis[J]. Chemom. Intell. Lab. Syst. 38, 223–242. https://doi.org/10.1016/S0169-7439(97)00031-2.
Paatero, P., Tapper, U., 2010. Positive matrix factorization: a non-negative factor model with optimal utilization of error estimates of data values. Environmetrics 5, 111–126. https://doi.org/10.1002/env.3170050203.
Pathak, R.K., Wu, W.S., Wang, T., 2009. Summertime $PM_{2.5}$ ionic species in four major cities of China: nitrate formation in an ammonia-deficient atmosphere. Atmos. Chem. Phys. 9, 1711–1722. https://doi.org/10.5194/acp-9-1711-2009.
Poirot, R.L., Wishinski, P.R., 1986. Visibility, sulfate and air mass history associated with the summertime aerosol in northern Vermont. Atmos. Environ. 20, 1457–1469. https://doi.org/10.1016/0004-6981(86)90018-1.
Polissar, A.V., Hopke, P.K., Harris, J.M., 2001. Source regions for atmospheric aerosol measured at Barrow, Alaska. Environ. Sci. Technol. 35, 4214–4266. https://doi.org/10.1021/es0107529.
Putaud, J.-P., Van Dingenen, R., Alastuey, A., Bauer, H., Birmili, W., Cyrys, J., Flentje, H., Fuzzi, S., Gehrig, R., Hansson, H.C., 2010. A European aerosol phenomenology-3: physical and chemical characteristics of particulate matter from 60 rural, urban, and kerbside sites across Europe. Atmos. Environ. 44, 1308–1320. https://doi.org/10.1016/j.atmosenv.2009.12.011.
Reff, A., Eberly, S.I., Bhave, P.V., 2007. Receptor modeling of ambient particulate matter data using positive matrix factorization: review of existing methods. J. Air Waste Manage. Assoc. 57, 146–154.
Seibert, P., Kromp-Kolb, H., Baltensperger, U., Jost, D.T., Schwikowski, M., 1994. Trajectory Analysis of High-Alpine Air Pollution Data. vol. 694, pp. 253–269. https://doi.org/10.1007/978-1-4615-1817-4-65.
Seinfeld, J.H., Pandis, S.N., 2006. Atmospheric chemistry and physics: from air pollution to climate change. Environ. Sci. Policy Sustain. Dev. 40, 26. https://doi.org/10.1063/1.882420.
Shen, Z.X., Wang, X., Zhang, R.J., Ho, K.F., Cao, J.J., Zhang, M.G., 2011. Chemical composition of water-soluble ions and carbonate estimation in spring aerosol at a semi-arid site of Tongyu, China. Aerosol Air Qual. Res. 11, 360–368. https://doi.org/10.4209/aaqr.2011.02.0010.
Shon, Z.H., Kim, K.H., Song, S.K., Jung, K., Kim, N.J., Lee, J.B., 2012. Relationship between water-soluble ions in $PM_{2.5}$ and their precursor gases in Seoul megacity. Atmos. Environ. 59, 540–550. https://doi.org/10.1016/j.atmosenv.2012.04.033.
Sievering, H., Boatman, J., Galloway, J., Keene, W., Kim, Y., Luria, M., Ray, J., 1991. Heterogeneous sulfur conversion in sea-salt aerosol particles: the role of aerosol water content and size distribution. Atmos. Environ. A. Gen. Top. 25, 1479–1487. https://doi.org/10.1016/0960-1686(91)90007-T.
Singh, R., Sharma, B.S., 2012. Composition, seasonal variation, and sources of PM_{10} from world heritage site Taj Mahal, Agra. Environ. Monit. Assess. 184, 5945–5946. https://doi.org/10.1007/s10661-011-2392-0.
Sirois, A., Bottenheim, J.W., 1995. Use of backward trajectories to interpret the 5-year record of PAN and O_3 ambient air concentrations at Kejimkujik National Park, Nova Scotia. J. Geophys. Res. Atmos. 100, 2867–2881. https://doi.org/10.1029/94JD02951.
Su, H., Pöschl, U., 2011. Soil nitrite as a source of atmospheric HONO and OH radicals. Science 333, 1616–1618. https://doi.org/10.1126/science.1207687.
Sun, Y., Jiang, Q., Wang, Z., Fu, P., Li, J., Yang, T., Yin, Y., 2014. Investigation of the sources and evolution processes of severe haze pollution in Beijing in January 2013. J. Geophys. Res. 119, 4380–4398. https://doi.org/10.1002/2014JD021641.
Sutton, M.A., Dragosits, U., Tang, Y.S., Fowler, D., 2000. Ammonia emissions from non-agricultural sources in the UK. Atmos. Environ. 34, 855–869. https://doi.org/10.1016/S1352-2310(99)00362-3.
Ta, W., Wang, T., Xiao, H., Zhu, X., Xiao, Z., 2004. Gaseous and particulate air pollution in the Lanzhou Valley, China. Sci. Total Environ. 320, 163–176. https://doi.org/10.1016/j.scitotenv.2003.08.026.
Tan, J.H., Duan, J.C., Chen, D.H., Wang, X.H., Guo, S.J., Bi, X.H., Sheng, G.Y., He, K. Bin, Fu, J.M., 2009. Chemical characteristics of haze during summer and winter in Guangzhou. Atmos. Res. 94, 238–245. https://doi.org/10.1016/j.atmosres.2009.05.016.
Ten Brink, H., Otjes, R., Jongejan, P., Slanina, S., 2007. An instrument for semi-continuous monitoring of the size-distribution of nitrate, ammonium, sulphate and chloride in aerosol. Atmos. Environ. 41, 2768–2779. https://doi.org/10.1016/j.atmosenv.2006.11.041.
Tolis, E.I., Saraga, D.E., Ammari, G.Z., Gkanas, E.I., Gougoulas, T., Papaioannou, C.C., Sarioglou, A.K., Kougioumtzidis, E., Skemperi, A., Bartzis, J.G., 2014. Chemical characterization of particulate matter (PM) and source apportionment study during winter and summer period for the city of Kozani, Greece. Cent. Eur. J. Chem. 12, 643–651. https://doi.org/10.2478/s11532-014-0531-5.
Trebs, I., Meixner, F.X., Slanina, J., Otjes, R., 2004. Real-time measurements of ammonia, acidic trace gases and water-soluble inorganic aerosol species at a rural site in the Amazon Basin. Atmos. Chem. Phys. Discuss. 4, 967–987. https://doi.org/10.5194/acp-4-967-2004.

Uematsu, M., Yoshikawa, A., Muraki, H., Arao, K., Uno, I., 2002. Transport of mineral and anthropogenic aerosols during a Kosa event over East Asia. J. Geophys. Res. Atmos. 107. https://doi.org/10.1029/2001JD000333 (AAC-1-AAC 3-7).

Usher, C.R., Michel, A.E., Grassian, V.H., 2003. Reactions on mineral dust. Chem. Rev. 103, 4883–4940. https://doi.org/10.1021/cr020657y.

Wang, F., 2014. Pollution Characteristics and Formation Causes of Atmospheric Particles and Its Chemical Components in Lanzhou City. (PhD thesis in Chinese). Lanzhou University, Lanzhou.

Wang, S., Yuan, W., Shang, K., 2006. The impacts of different kinds of dust events on PM pollution in northern China. Atmos. Environ. 40, 7975–7982. https://doi.org/10.1016/j.atmosenv.2006.06.058.

Wang, X., Xia, D., Wang, T., Xue, X., Li, J., 2008. Dust sources in arid and semiarid China and southern Mongolia: impacts of geomorphological setting and surface materials. Geomorphology 97, 583–600. https://doi.org/10.1016/j.geomorph.2007.09.006.

Wang, Y.Q., Zhang, X.Y., Draxler, R.R., 2009. TrajStat: GIS-based software that uses various trajectory statistical analysis methods to identify potential sources from long-term air pollution measurement data. Environ. Model. Softw. 24, 938–939. https://doi.org/10.1016/j.envsoft.2009.01.004.

Wang, X., Hua, T., Zhang, C., Lang, L., Wang, H., 2012. Aeolian salts in Gobi deserts of the western region of Inner Mongolia: gone with the dust aerosols. Atmos. Res. 118, 1–9. https://doi.org/10.1016/j.atmosres.2012.06.003.

Wang, L., Du, H., Chen, J., Zhang, M., Huang, X., Tan, H., Kong, L., Geng, F., 2013. Consecutive transport of anthropogenic air masses and dust storm plume: two case events at Shanghai, China. Atmos. Res. 127, 22–33. https://doi.org/10.1016/j.atmosres.2013.02.011.

Wang, Y., Jia, C., Tao, J., Zhang, L., Liang, X., Ma, J., Gao, H., Huang, T., Zhang, K., 2016. Chemical characterization and source apportionment of $PM_{2.5}$ in a semi-arid and petrochemical-industrialized city, Northwest China. Sci. Total Environ. 573, 1031–1040. https://doi.org/10.1016/j.scitotenv.2016.08.179.

Weber, R.J., Kapustin, V., Clarke, A., 2005. Dust composition and mixing state inferred from airborne composition measurements during ACE-Asia C130 Flight #6. Atmos. Environ. 39, 359–369. https://doi.org/10.1016/j.atmosenv.2004.08.046.

Whitehead, J.D., Longley, I.D., Gallagher, M.W., 2007. Seasonal and diurnal variation in atmospheric ammonia in an urban environment measured using a quantum cascade laser absorption spectrometer. Water Air Soil Pollut. 183, 317–329. https://doi.org/10.1007/s11270-007-9381-5.

World Health Organization (WHO), 2014. Ambient (outdoor) air pollution in cities database 2014. http://www.who.int/phe/health_topics/outdoorair/databases/cities/en/.

Xue, J., Lau, A.K.H., Yu, J.Z., 2011. A study of acidity on $PM_{2.5}$ in Hong Kong using online ionic chemical composition measurements. Atmos. Environ. 45, 7081–7088. https://doi.org/10.1016/j.atmosenv.2011.09.040.

Ye, Z., Liu, J., Gu, A., Feng, F., Liu, Y., Bi, C., Xu, J., Li, L., Chen, H., Chen, Y., 2016. Chemical characterization of fine particulate matter in Changzhou, China, and source apportionment with offline aerosol mass spectrometry. Atmos. Chem. Phys. 17, 1–46. https://doi.org/10.5194/acp-17-2573-2017.

Zeng, Y., Hopke, P.K., 1989. A study of the sources of acid precipitation in Ontario, Canada. Atmos. Environ. 23, 1499–1509. https://doi.org/10.1016/0004-6981(89)90409-5.

Zhang, D., Iwasaka, Y., Shi, G., Zang, J., Hu, M., Li, C., 2005. Separated status of the natural dust plume and polluted air masses in an Asian dust storm event at coastal areas of China. J. Geophys. Res. Atmos. 110, D06302. https://doi.org/10.1029/2004JD005305.

Zhang, X.L., Wu, G.J., Zhang, C.L., Xu, T.L., Zhou, Q.Q., 2015. What's the real role of iron-oxides in the optical properties of dust aerosols? Atmos. Chem. Phys. 15, 5619–5662. https://doi.org/10.5194/acpd-15-5619-2015.

Zheng, X., 1991. Salt lakes on the inner Mongolian plateau of China. Chin. Geogr. Sci. 1, 83–94. https://doi.org/10.1007/BF02664459 (in Chinese).